Investigation of undesired errors relating to the planar array system of electrical impedance mammography for breast cancer detection

By Rabia Bilal

A Thesis submitted for the degree of Master of Philosophy

Biomedical Engineering, School of Engineering and Informatics

University of Sussex

March 2012

Declaration

I hereby declare that this thesis has not been submitted, either in the same or different form, to this or any other University for a degree and the work produced here is my own except stated otherwise.

Sign: .....

Rabia Bilal

Date: 03/04/2012

Abstract

Breast cancer in women continues to be one of the leading causes of death in the world. Since the exact causes are not completely known, the most important approach is to reduce this mortality by early detection and treatment. Although the current detection techniques for breast cancer such as X-ray mammography provide useful information for diagnosis; development of a new imaging technique using non-ionising radiation is highly desirable in order to detect breast cancer at an early stage and overcome current limitations, such as age-dependent sensitivity. Electrical Impedance Mammography (EIM) provides a new solution to break through the current limitation for early cancer detection.

The focus of this thesis is to investigate the current fourth generation Sussex EIM system. This system implements the EIM technique by examination of the tissue response to a multi-frequency injected current. The Sussex Mk4 system is discussed in detail followed by system hardware modelling. The hardware modelling includes both analogue and digital components. The analogue part includes modelling of the voltage to current converter (V-I) and analogue multiplexer while the digital section consists of modelling the signal generation, measurement and demodulating components. In the analogue section, bandwidth limitation due to the current source and the analogue multiplexer's configuration is also the prime focus of investigation along with the proposal to overcome it.

Possible factors affecting the system performance and signal quality are also part of the research. In this section, possible factors are characterized and discussed in detail on the basis of external and internal sources of possible errors along with predictable and unpredictable noise sources. External sources of error artefacts introduced by the patients and their movements while scanning are most likely to affect the image reconstruction. Predictable and unpredictable causes may introduce frequency dependent noise whereas internal sources, which can be also be classified as systematic errors, degrade system performance due to electronic circuit design, configuration, stray capacitance and cable connections.

Further, comprehensive investigation is performed on the *in-vivo* undesired voltage threshold levels which come hand-in-hand with the methods to mitigate the possible factors responsible for them. A comprehensive study and analysis is also carried out to determine what ratio of electrode blockage can affect the acquired raw data and how this may compromise reconstruction. Techniques for fast detection of any such occurrences are also discussed.

Acknowledgement

I would like to express my profound gratitude to my supervisors, Dr Rupert Young and Dr Wei Wang for their kind support, encouragement and guidance which enabled me to attain this thesis.

My sincere gratitude also goes to Prof Chris Chatwin for his sincere guidance, motivation and encouragement which enriched every step on the road to the completion of the research project.

I am forever indebted to my parents, Najma and Shakoor. They raised, loved , taught and made me what I am today.

Most importantly, I wish to thank you my soul mate, Bilal for standing by me, companion, Mustafa ,best friend, Amina and brother Shehreyar for their understanding, endless patience, love and support.

Table of Contents

List of Figures

List of Tables

List of Abbreviations

2-D	Two-dimensional
3-D	Three-dimensional
A.C.	Alternating current
ADC	Analogue to digital converter
API	Application programming interface
C	Cell membrane capacitance
C_{ON}	Switch ON capacitance
C_{OFF}	Switch OFF capacitance
CS	Current source
DA	Differential amplifier
DAC	Digital to analogue converter
D.C.	Direct current
APT	Applied potential tomography
dB	Decibel
EIM	Electrical impedance mammography
EIT	Electrical impedance tomography
EM	Electromagnetic
Im(Z)	Imaginary part of impedance(reactance)
KHz	Kilohertz
LPF	Low pass filter
MHz	Megahertz
Mk	Mark
MRI	Magnetic resonance imaging
MUX	Multiplexer
NI	National Instrumentation
R_{ON}	Switch ON resistance
Re(Z)	Real part of impedance (resistance)
SNR	Signal to noise ratio
V_{p-p}	Peak to peak voltage
V-I	Voltage to current

List of Symbols

α	Cole distribution constant
f	Frequency under investigation
F_r	Dispersion frequency
R	Extracellular resistance
R_o	Impedance at very low frequency
R_∞	Impedance at very high frequency
S	Intracellular resistance
Z	Impedance

Chapter 1 Introduction

1.1 Introduction

In order to understand the use of Electrical Impedance Mammography (EIM) in the detection of breast cancer in the early stages a number of areas must be researched. This chapter presents a brief introduction of breast cancer, bio impedance basics, current available detection technologies and clinical applications.

A description of the aims and objectives of the research with an outline of the thesis is given below.

1.2 Breast cancer anatomical background

Breast cancer is a significant healthcare problem and the second leading cause of death in women worldwide for the past two decades (American Cancer Society 2009, Ferlay *et al* 2010).

Cancer is very difficult to diagnose in its early stages and patients only experience the symptoms when cancer has fully developed. As yet there are no effective cancer detection techniques that can detect and cure cancer at an early stage.

Cancer is a disease of cells which are the tiny building blocks making up the organs and tissues of the body. Normally, cell production takes place in an orderly and controlled manner. If, for some reason, the process gets out of control, the cells will continue to divide, finally developing into a lump called a tumour (Knowles and Selby 2005).

Tumours can either be benign, in situ carcinomas or malignant (Knowles and Selby 2005). In a benign tumour the cells do not spread to other parts of the body and so are not cancerous. In situ carcinomas have similar cell structure to that of the cancer cells but remain in the epithelial layer. A malignant tumour consists of cancer cells which have the ability to spread beyond the original site. If left untreated they may invade and destroy surrounding tissues. Sometimes cells break away from original (primary) cancer and spread to other organs in the body through the blood stream or lymphatic system.

When these cells reach a new site they may go on dividing and form a new tumour, often referred to as a secondary or metastasis.

The term breast cancer refers to a malignant tumour that has developed from cells in the breast. The breast is composed of two main types of tissues: glandular tissues and stromal (supporting) tissues. Glandular tissues house the milk-producing glands (lobules) and the ducts (the milk passages) while stromal tissues include fatty and fibrous connective tissues of the breast. The breast is also made up of lymphatic tissue-immune system tissue that removes cellular fluids and waste.

The most common types of breast cancer arise from either the ducts or the lobules. Ductal carcinoma, the most common type (80% of all breast cancers), is found in the cells of the ducts and usually forms a hard lump (Breast.Net Jan 2004). Carcinoma of the breast lobules has the second highest rate, about 10%-15%. The rest are rare forms of cancers, for example of the connective tissues (Breast.Net Jan 2004).

1.3 Breast cancer stages:

The stage of cancer defines its size and spread beyond its original site. Generally breast cancer is divided into five stages from a very early form (stage 0) to spreading to other parts of the body (stage 4) (Knowles and Selby 2005, http://www. breastcancer.org).

Stage 0: Non-spreading into the surrounding breast tissues; these may also be referred to as non invasive stage.

Stage 1: less than two centimetres; the lymph glands in the armpit are not affected and there are no signs that the cancer has spread elsewhere in the body.

Stage 2A and 2B: between two and five centimetres, or the lymph glands in the armpit are affected, or both; however, there are no signs that the cancer has spread further.

Stage 3A ,3B and 3C: larger than five centimetres and may be attached to surrounding structures such as the muscle or skin; the lymph glands are usually affected, but there are no signs that the cancer has spread beyond the breast or the lymph glands in the armpits.

Stage 4: any size; but the lymph glands are usually affected and the cancer has spread to other parts of the body. This is secondary breast cancer.

1.4 Survival rates

Mortality rate of the disease can be reduced by detecting the cancers in their early stages. Breast cancer detected at an early stage has very high survival rates, which are up to 90% after 5 years and almost 88% after 10 years. Later stage detections decrease the survival rates to approximately 13% after 5 years and less than 10% after 10 years. Therefore, the earlier the stage that cancer diagnosis occurs the higher the survival rates for the patients (Cancer Research UK between 1990 and 1994 followed up to end of 2004).

1.5 Current cancer detection techniques

Early cancer detection challenges very much rely on diagnostic imaging techniques at the screening stage. Surgical procedures such as needle biopsy and core biopsy along with imaging techniques assist each other during cancer diagnosis. Biopsy samples help in diagnosis of the cancer stage and imaging techniques help to locate the cancer regions in the body (http://www.nationalbreastcancer.org).

1.5.1 Self examination

In many cases the main way in which breast cancer is first detected is self-examination by the patient. The presence of breast cancer may cause several physical changes in or on the breast which may be detected by the woman herself. These changes can take the form of a lumpy feeling to the breast, a change of the skin (sometimes a dimpling or indentation), a change to the nipple which may become pulled-in or start to discharge, a swelling of the breast with the skin becoming red or sometimes like an orange peel, or sometimes a patient will have a lump under their armpit due to breast cancer which has spread to the lymph nodes.

The following section lists other biomedical techniques in use to detect the presence of breast tumours and to confirm if they are malignant or benign.

1.5.2 X-ray mammography

X-ray imaging involves passing a beam of X-rays through the body and onto a plate containing a film which is sensitive to X-rays (Margie *et al* 2001). Due to the varying density of human tissues the resulting image on the film will be related to the tissue density within the part of the body being imaged. This works very well with bones and other high density organs since the difference in density compared with surrounding tissues produces a high contrast image. However, in younger women the breast tissue is denser and this can make it difficult to detect any changes on the mammogram since normal breast tissue is of similar density to cancerous tissue.

Therefore, X-ray mammography is usually used for women over the age of 35 (www.medicinenet.com). Firstly, the breast is pressed as flat as possible between two plates. Then an x-ray image is formed in the usual way.

1.5.3 Ultrasound scans

Ultrasound imaging (Entrekin *et al*1999) works by transmitting high frequency acoustic energy into the body via an ultrasound transmitter and recording the reflected wave fronts. Reflections occur wherever there is a change in density that gives rise to stronger reflections, and the depth of the density change is calculated from the time taken between the pulse being transmitted and the recorded echo. One of the benefits of ultrasound imaging is its ability to diagnose whether a lump is solid or fluid-filled (i.e. a cyst).

1.5.4. Magnetic resonance imaging (MRI)

Magnetic resonance imaging (Kopans D.B. 1998) uses a strong magnetic field coupled with a series of rapidly varying electromagnetic fields to build up images relating to the proton density within the atoms that make up the cells in the body. The patient has to be positioned inside a tunnel from around which the magnetic and electromagnetic fields are applied. Sometimes a contrast-enhancing agent (Gadolineum-Diethelene-Triamene-Pentaacetic Acid or Gd-DTPA) is injected into the blood to improve the image. The image may also be improved by using what are known as 'surface coils' to enhance the detection of the electromagnetic fields emitted from the particular part of the body being imaged. There are numerous parameters which may be altered through the application of the electromagnetic fields in order to make the images sensitive to different tissue types. At present MRI is mainly used in solving some specific breast problems such as the evaluation of silicone implant rupture, distinguishing scar from cancer recurrence and local staging of breast cancer. Additionally, the imaging process is very time consuming and the cost of MRI imaging is higher than that of X-ray mammography. These facts mean that the technique is not appropriate for routine screening.

1.5.5 Needle tests and biopsies

Normally further surgical procedures are required to determine the exact nature of the abnormality after imaging screening. These include fine needle aspiration (FNA) and core biopsy FNA which consist of a small needle being inserted into the lesion to remove fluid, in the case of a cyst, or a small number of cells for histological analysis. Core biopsy is similar except that the procedure is carried out using a much wider bore needle. Local anaesthesia is used and the removed cells are similarly analysed. In cases where the lump is too small to feel through the skin, the needle may be guided with the help of X-ray or ultrasound images into the site of the abnormality.

1.5.6 Infrared Thermography

Breast thermography uses digital infrared thermal imaging to make diagnostic quality images of the breast. Thermology is a medical science that diagnoses cancer from infrared images of the breast. Breast thermography is totally non invasive and radiation energies are not sent into the body. It works on the principle that all things above absolute zero emit infrared energy. The thermal imaging camera captures this energy and converts it into an image that can be viewed on a computer.

It is very important to appreciate that thermography does not replace mammograms. It is used in connection with mammograms and gives the opportunity to make decisions with as much information as possible (Head *et al* 1988).

1.6 Cancer treatment methods

There are three primary treatments available for the detected cancer in light of the cancer stage. The recovering rates of the three methods discussed below are approximately 49% by surgery, 40% by radiotherapy and 11% by chemotherapy (Tobias *et al* 2010).

1) Surgery
2) Radiotherapy
3) Chemotherapy

1.6.1 Surgery

Local cancers are removed by surgery. Cancers which are not suitable or have residuals from surgery are treated with radiotherapy and chemotherapy.

1.6.2 Radiotherapy

In radiotherapy, ionizing radiation is utilized to treat cancer tissues by damaging the DNA of malignant cells using radiation exposure. This will consequently stop the cell cycle of cancer cells and force them into apoptosis (programmable cell death). To reduce the side effects of radiotherapy, a precise imaging technique, MRI, is commonly required to provide accurate location of the radiation region to avoid involving, as far as is possible, normal surrounding tissues.

1.6.3 Chemotherapy

In chemotherapy, anticancer drugs, containing cyto toxic pharmaceutical compounds, are given to the patient. Similar with mechanisms induced by radiotherapy, cyto toxic drugs produce their effects by damaging DNA or by blocking the cell cycles at certain points, such as the S and M stages (Knowles and Selby 2005). Again, the side effects and drug resistance of cancers are common and reduce the effectiveness of chemotherapy treatments.

1.7 Aims and Objectives

The aim of the research project is to focus on the performance and data quality affecting factors of the current fourth generation Sussex EIM system. The analogue section bandwidth limitation due to the current source and the analogue multiplexer's configuration is going to be investigated along with the proposal to overcome it.

Possible factors affecting the system performance and signal quality are to be characterized and discussed in detail on the basis of external and internal sources of possible errors along with predictable and unpredictable noise sources. External sources of error artefacts introduced by the patients and their movements while scanning are most likely to affect the image reconstruction. Predictable and unpredictable causes may introduce frequency dependent noise whereas internal sources, which can be also classified as systematic errors, degrade system performance due to electronic circuit design, configuration, stray capacitance and cable connections.

A further aim is to investigate the possible mitigating methods for the above mentioned errors so as to reduce and improve the signal quality and image reconstruction.

1.8 Achievements

Several of the research achievements of the thesis are summarised as follows:

A system performance analysis is made of electronic hardware to generate signals for injection into tissue. The acquisition system needs to have a good signal-to-noise ratio and perform linearly over a wide bandwidth.

Characterisation is made of potential in-vivo artefacts that might affect the system performance and image quality for medical diagnosis. Artefacts are categorized as external and internal sources.

Internal sources of errors limiting system bandwidth are overcome by the suggested multiple voltage to current converter configurations used with the analogue multiplexers.

Comprehensive investigation of possible artefacts blocking the planar electrodes is carried out defining what ratio of electrode blockage can affect the acquired signal quality more.

Methods to mitigate the investigated artefacts are devised to improve image quality and system performance. This section includes a fast sweep method to detect any electrode blockage due to the patient's skin or any debris.

1.9 Outline of the thesis

The aim of this research is to evaluate and optimize the current Mk4 EIM system hardware performance to obtain higher quality system performance over a wide bandwidth. This investigation is followed by the possible factors affecting in-vivo system performance and image quality.

These distinct research areas are grouped into separate chapters.

This introductory chapter presents the aims and objectives of this research and the main achievements.

Chapter 2 provides a review of breast cancer discusses the shortcomings of the current detection techniques and identifies the need for new, safer and cheaper detection techniques. Provides an overview of the Electrical Impedance mammography history and emphasizes its benefits for the early stage detection of breast cancer.

Chapter 3 gives an overview of the Sussex EIM system along with the hardware system model.

Chapter 4 discusses the contributing sources of artefacts limiting system performance and image quality of Sussex planar array system

Chapter 5 Investigates the undesired voltage threshold levels observed during acquired data analysis.

Chapter 6 Methods to detect and mitigate infinite impedance possibilities to improve the system performance and image quality.

Chapter 7 presents the conclusions of this study and some suggestions for future work.

Chapter 2 Overview of EIM Technique

2.1 Introduction

As discussed previously, the earlier the breast cancer is detected the higher the survival rate is. The current diagnosis techniques are deficient in early detection, especially for younger women. A relatively new diagnosis technique based on Electrical Impedance Mammography (EIM) could overcome some of the problems identified and is under investigation.

This chapter introduces EIM technique, overviews its clinical applications and then discusses its application for breast imaging. The characteristics of EIM are then presented together with an in depth discussion of tissue modelling. At the end of the chapter, a summary of the EIM technique is presented.

2.2 Electrical Impedance Tomography (EIT)

2.2.1Brief review of EIT

Electrical Impedance Tomography (EIT) was developed since early 1980s (Barber and Brown 1982). It estimates the electrical impedance properties of the interior of an object from measurements made on its surface (Barber and Brown 1995). It is based upon specific transmission of electrical currents due to specific conductivity and permittivity of regions of the object. EIT measurements are typically performed by injecting small currents through electrodes around the region to be imaged with the resulting potentials measured between pairs of electrodes. These potentials are then used to reconstruct the conductivity of the imaged region. With a prior knowledge of the conductivity of various components comprising the image region, the composition of the structure can be determined.

It is possible to apply this new technique on human beings because the electrical impedance of different body tissues varies widely from 0.65 Ω.m for cerebrospinal fluid to 150 Ω.m for bone (Medical imaging research 2004). Since electric currents applied to the body depend on the tissue's conductivity distribution, organ interior images can be reconstructed from the data acquired on the surface of the body.

Figure 2.1 illustrates a block diagram representation of an EIT system. It usually consists of four major parts: signal generation, data acquisition, system, image reconstruction & image display and data analysis.

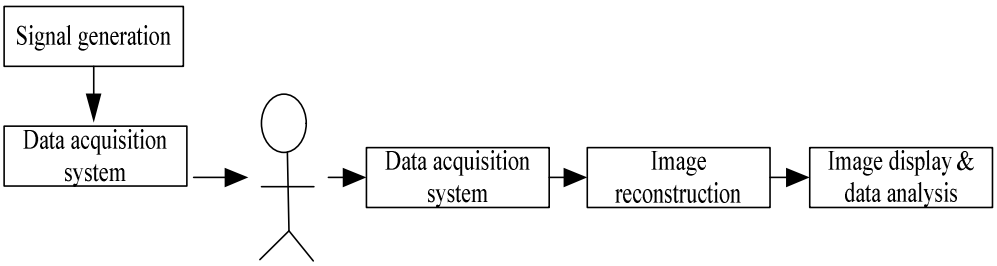

Figure 2.1 Block diagram of EIT system

2.2.2 Types of EIT

In a typical EIT system, currents are injected into the object and the voltages are measured through electrodes on the surface. According to the method of current injection, there are two types of EIT system.

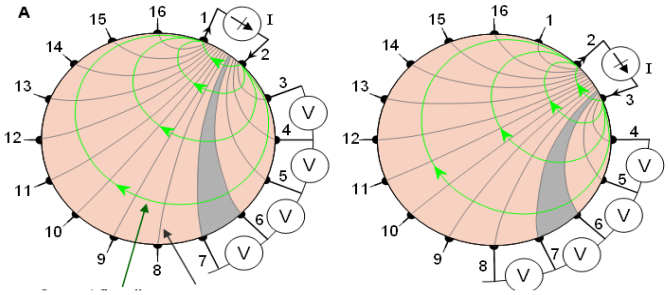

(a) (b)

Figure 2.2 Single current source of impedance data collection (Impedance tomography Jan 2004)

The first type, used by the Sheffield group, was called Applied Potential Tomography (APT) until the late 1980s and then called EIT (Brown and Seagar 1987, Smith *et al* 1990, Barber *et al* 1992, Sinton *et al* 1992). This kind of system sequentially applies electrical currents to the object using a pair of adjacent electrodes. While current is applied to the object, voltages between adjacent noncurrent carrying electrodes are

measured and this procedure is repeated for all electrodes. Then each applied current between a pair of adjacent electrodes obtains a voltage data set, one of which is used as a reference data set. Once another voltage data set is measured, the voltage difference between this new set and the reference set along isopotential contours of the reference medium can be calculated. Using a proper reconstruction algorithm, images showing data corresponding to changes in the electrical characteristics of the object are displayed (Barber *et al* 1992). Figure 2.2 shows a simple measurement procedure with 16 electrodes. The current is first applied through electrodes 1 and 2 as shown in Figure 2.2(a). The current density is, of course, highest near these electrodes, decreasing rapidly as a function of distance.

The voltage is measured successively with electrode pairs 3-4, 4-5,….15-16. From these 13 voltage measurements the first four measurements are shown in Figure 2.2(a).The next set of 13 voltage measurements are obtained by injecting the current through electrodes 2 and 3, as shown in Figure 2.2 (b). For a 16-electrode system, 16*13 = 208 voltage measurements are obtained (Impedance tomography Jan 2004).

The other current injection type is “Adaptive Current Tomography (ACT)” (Gisser *et al* 1998, Edic *et al* 1993, Cook *et al* 1994, Zhu *et al* 1994, Edic *et al* 1995) which simultaneously applies electrical currents to all electrodes. A number of current patterns are applied, where each pattern defines the current for each electrode, and the subsequent electrode voltages are measured to generate the data required for image reconstruction. In the ACT method, the current is injected through all electrodes illustrated in Figure 2.3(a), since current flows through all electrodes used for different current distributions. The voltages are measured with respect to a single grounded electrode. When 16 electrodes are used, the number of voltage measurements of a certain current distribution is 15.The desired current distribution is then rotated one electrode increment as shown in Figure 2.3 (b). Thus 8 different current distributions are obtained, yielding 8*15 = 120 independent voltage measurements (Impedance tomography, Jan 2004). The disadvantage of the ACT system is to increase hardware complexity since it requires variable current sources for each electrode, rather than a single source driving one pair of electrodes at a time(Saulnier *et al* 2001).

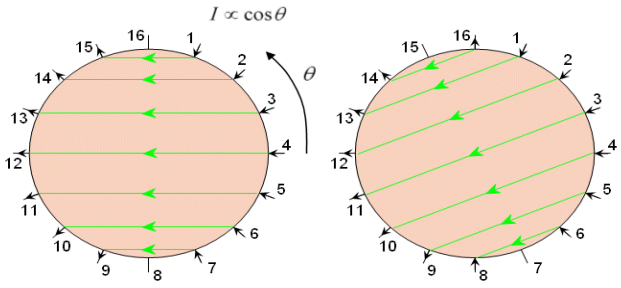

(a) (b)

Figure 2.3 Multiple current sources method of impedance data collection (Impedance tomography, Jan 2004).

2.2.3 History of EIT

Cole and Cole provided the first model of tissue impedance characteristics in 1941 (Cole and Cole 1941).This Cole-Cole model is still widely used today.

The first impedance image obtained with the modern EIT technique was published by Henderson and Webster (Henderson and Webster 1978) in 1978. However, they produced trans-thoracic impedance images of the thorax rather than real tomography images.

The inventors of the first imaging EIT system were Barber and Brown of the University of Sheffield (UK) in 1982 (Barber and Brown 1982).This was, for the first time, a real two-dimensional impedance image display produced by an impedance measurement system, which employed 16 electrodes in its data collection system and used a back projection based image reconstruction algorithm. The data collection was performed in real time at a speed of 10 frames per second. It was a serial configuration with 16 current drivers and 16 voltage receivers acquiring at a frequency of 50 kHz. The overall accuracy of the data collection system was about 1 %(Barber *et al* 1983, Barber and Brown 1984).

Since that time, research on EIT systems, image reconstruction algorithms and applications has developed rapidly for animals and humans, both in-vitro and in-vivo (Boone and Holder 1996, Brown 2003, Zou and Gou 2003, Lionheart 2004, Bayford 2006). The frequency band used also varied widely with measurements being taken in the range of a few hertz to that of microwaves. The first results were presented at the

European Community Workshops on Electrical Impedance Tomography in Sheffield, UK and Lyon, France in 1986 and 1987, respectively. Annual EPSRC Network Meetings on EIT were held in UCL, London from 1999 to 2001 and there was an EIT workshop in the USA in August 2002.

2.3 Clinical applications of electrical impedance tomography

2.3.1 Thorax

Since 1982, Barber and Brown have designed a prototype system suitable for clinical use to detect changes in intra thoracic fluid volumes (Barber and Brown 1982). All recordings made using the Sheffield Mark 1 system were with a 16 electrode array placed around the lower thorax. Ten patients were studied during the sequential aspiration of unilateral pleural effusions. Following recording of a baseline data set during tidal breathing (600 cycles) fluid was aspirated in 300ml aliquots up to a maximum of 1000ml, 600 cycles of data being collected after each aspiration. On the side of the effusion there was a progressive increase in inter thoracic impedivity per 100ml by 7% and the range was 3%-13%. In the contra lateral lung there was a smaller increase in all subjects (mean 1.8%, range 1%-3%) consistent with a reduction in meditational shift following aspiration (Campbell *et al* 1994).

Zhao and Nopp (Zhao *et al* 1996, Nopp *et al* 1996) reported the study of small regions of interest (ROI) on the thorax images formed by the Sheffield MK3 EIT system. They successfully studied the cardiac changes in lung impedivity as a function of frequency and location, and conducted modelling of cardiac related changes in lungs, which is based on a 2-D EIT system. However, it was found that it was difficult to define some cardiac regions, for example, ventricle and aorta etc., due to the low resolution of the EIT system.

2.3.2 Brain

A series of studies in this field has shown that impedance changes caused by physiological events within the brain may be large enough to enable an injected current EIT system to produce reasonable images of the variations. In 1992, Holder (Holder

1992, Holder 1993) observed an impedance increase of 20%-200% during global cerebral ischemia and cortical spreading depression in the rat when using cortical electrodes. In addition, EIT was used to produce impedance images of sensory and visually evoked responses in the rabbit brain that showed impedance decreases of 4.5.% ± 2.7% and 2.7% ± 2.4%, respectively.

Tower (Towers *et al* 1999) developed a 3-D finite element model of the human head. Simulations were performed to calculate the effect of impedance changes due to auditory evoked responses and the application of a carotid clamp on the electrode pair potential differences. These examples were chosen to represent a wide range of possible impedance variations within the human head. The results from the simulations predicted that these two cases caused fractional changes of between 10^{-6} and 10^{-5} in the majority of the electrode pair potential differences. Consequently, in order to detect a variety of impedance changes within the human head, an EIT system incorporating diametric current injection would require a sensitivity in the range 100-120dB (Tidswell *et al* 2001,McEwan *et al* 2006).

Gongalves (Gongalves *et al* 2003) obtained the in-vivo measurement data of impedance of skull and brain using an EIT method.

These researchers focused on medical applications and have shown that the EIT technique can be used in the clinical environment to detect small changes at the tissue level.

2.4 Electrical impedance mammography

Electrical Impedance Mammography (EIM) is an important application of the Electrical Impedance Tomography technique for human breast imaging. A number of research groups around the world, including a pioneering group at the University of Sussex, have been researching in this field since 1996, previously in University of De Monfort.

2.5 Review of some existing EIM Systems

2.5.1 Dartmouth EIM System

The EIM imaging system at Dartmouth College (Hartov *et al* 2000) uses an annular ring of 32-electrodes. The electrode driving circuitry can be operated as either a voltage or a current source, and there is a dedicated drive channel for each electrode. The input to each drive channel is supplied by a waveform generator with a frequency range from 1 kHz to 1MHz and the input amplitude to each channel can be individually programmed. Thus it is possible to drive current through all electrodes simultaneously with fully programmable patterns. The amplitude of the sampled signal is recovered using a digital phase-sensitive detection technique, which allows both real and imaginary components to be measured. The Dartmouth system is quoted to have a frame rate of 0.22 image/sec. The signal-to-noise ratio performance is 75dB. Image reconstruction is performed using the Newton-Raphson method to optimise a conductivity distribution modelled by a pair of finite element meshes.

2.5.2 Moscow EIM System

The system developed by Cherepenin (Cherepenin *et al* 2002) uses a planar array consisting of 256 electrodes obtaining images of the three dimensional conductivity distributions in regions below the skin's surface up to several centimetres deep. Using the developed measuring system and image reconstruction algorithm, examples of tomography images were obtained in vivo during clinical tests. The mammary gland, being an organ-target, alters with such physiological events as menstrual cycle, pregnancy, lactation and post menopause. They estimated the possibilities of the EIM technique for investigation of mammary gland state among women with different hormonal status and found that electrical impedance mammograms from different groups had clear visual distinctions and statistically significant differences in mammary gland conductivity. The data on conductivity distribution in the mammary gland during different physiological periods have been measured as well.

2.5.3 Sussex EIM System

The current Mk4 EIM system has been developed for breast imaging since 1996. The current source circuitry is driven by 1V voltage from the National Instruments (NI) function generator and is designed to supply a 1mA current over a frequency range of 1 kHz to 5 MHz. The current is injected through two electrodes via fully programmable analogue multiplexers in a planar electrode system.

The surface voltages are switched serially via the multiplexers to the measurement circuitry. Digital demodulation is then applied by the NI ADC board with the final imaging performed by a host PC.

2.6 Characteristic of EIM

2.6.1 Advantages of EIM technique

As an emerging medical imaging technique, EIM has many advantages in the detection of breast cancer.

1) Early detection

   Different types of tissue have different electrical properties. Even the same type of tissue when under different physiological condition may have different electrical properties (Cole 1941, Foster 1989). EIM is a functional imaging method which has the potential to show physiological and pathological information. Theoretically, it is able to find the smallest changes in the body. Particularly, it has the capacity to detect abnormal tissue such as cancerous tissue from normal tissue. Therefore, with this technique, earliest detection of cancer at the non-invasive stage (stage 0) might be possible.

2) No patient age limit

   Despite of the low risk of breast cancer in women under the age of 40, the incidence has been increasing in this age group. Breast cancer in young women is tending to be more aggressive than in older women. Also, their dense breast tissue may make X-ray mammography more difficult to read and interpret. EIM is thus a pioneering means for breast cancer to provide an effective tool for

detecting carcinoma in young women before the disease becomes life threatening.

3) Non-invasive and no radiation

   EIM does not require exposure to ionizing radiation. It uses tiny injected currents and is harmless to patients and operators. As compared with X-ray mammography in which the breast is compressed to produce a clearer image and a small biopsy needle is, in addition, inserted into the located lesion, EIM uses non-invasive measurement for patients.

4) Low cost and convenient

   Due to the simple hardware system, EIM is much cheaper and faster than techniques such as computerised X-ray mammography and positron emission mammography.

5) Broad clinical applications

   The electrical properties of human tissue change when the current frequency changes (Gabriel 1996). Every type of tissue corresponds to an impedance spectrum, which could possibly be used as a fingerprint to characterise and identify different tissues. It has invaluable prospects for medical clinical applications.

2.6.2 Current limitations of the EIT technique

When applying the EIM technique to clinical diagnosis, a major problem is the limitation of its poor spatial resolution. The image quality is mainly related to two factors: the accuracy of the data collection system and the image reconstruction technique.

The correct information from the data collection system is determined not only by the number of electrodes used and electrode configuration but also the applied current patterns and voltage measurement strategy (Barber 1994). In particular, the numbers of electrodes are very important for data acquisition and image reconstruction. However, it

is not a case of simply increasing the number of electrodes to improve the quality of information. This is due to the practical difficulties of applying large numbers of electrodes to the body, the associated complexity of accurately measuring signals with large dynamic range and computational difficulties of processing vast quantities of data in a reasonable time (Seager *et al* 1987).

Additionally, image reconstruction is much more difficult than that of other modalities, such as X-ray. In EIT, the reconstruction algorithm uses knowledge of the applied current patterns and the measured electrode voltages to solve the inverse problem, computing the electrical impedance distributions in the object. The current flow is determined by the impedance distribution within the object in contrast to the photon paths in an X-ray which are essentially straight lines. Furthermore the inverse problem is said to be ill posed, meaning that large changes in impedance distribution in the interior of the object can result in only small voltage changes at the surface. However, some new algorithms, such as Genetic algorithms (Kim *et al* 2002), to improve the spatial resolution of EIT images are under study and have revealed relatively good performance.

2.7 Modelling and factors affecting human tissue and cells

2.7.1 Human tissue modelling

The breast is formed from various tissue types but it has a high content of fatty tissue known as adipose. It is necessary to go beyond the organ and even beyond the tissue; in fact it must be observed from the point of view of its cellular structure. The advantage with looking at the breast at the cellular level is that all human cells, although organised in different ways with different DNA expressions for varying tissues, have the same structure and can be modelled in the same way.

2.7.2 The tissue model

The basic principles of EIT rely on the frequency response of cells. At higher frequencies the current path is directly through the cell membrane. At lower frequencies the current flows outside the cells in the inter-cellular fluid.

2.7.3 Mathematical modelling of human tissue and cells

Human tissue consists of cells within a conducting medium; the cells are separated from the conducting medium by an electrically insulated cell membrane. This cell acts like a capacitor between the inter- and intra-cellular medium. Electrical representation of human tissue based on a simple 3 element model is shown in Figure 2.4 below, originally proposed by Cole and Cole (Cole and Cole 1941).

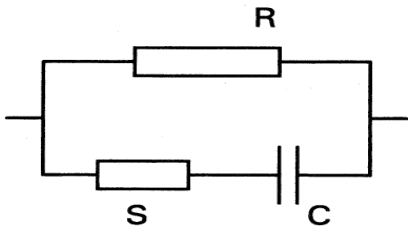

Figure 2.4 Electrical model for a human tissue.

In the model:

R is the extracellular resistance,

S is the intracellular resistance and

C is the cell membrane capacitance.

At lower frequencies the overall impedance is dominated by R because C has high impedance. At higher frequencies overall impedance will be R in parallel with S. This model is too simple and an actual tissue would be better represented as a large network of interconnected modules of this form.

Cancer has lower impedance than the normal tissues (Smith *et al* 1986, Surowiec *et al* 1988, Jossinet 1996, Brown *et al* 2005). The extra cellular electrical property of cancer is usually lower than that of healthy tissue due to the changes in cell density. The cancer extra cellular property is mainly detected at low frequencies. Moreover, cancer cell membrane has relatively low membrane capacitance as compared to normal cells (Han *et al* 2007) which can be modelled as:

$$Z = R_\infty + (R_0 - R_\infty) \Big/ \left[1 + \left(j_f / F_r\right)^\alpha\right] \qquad (2.1)$$

R_0 is the low frequency limit resisitivity, R_∞ is the high frequency limit resistivity, α is a dimensionless numerical constant called the relaxation factor and has a value between 0 and 1(Mc Adams *et al* 1995).

At very low frequencies of applied current, the current cannot pass through the membrane, and conduction is through the extracellular space, R. So $R_0 = R$. At high frequencies, current can flow through the membrane, which act as capacitors. The equivalent circuit representation is R in parallel with S (see figure 2.5 below). So $R_\infty = RS/(R+S)$.

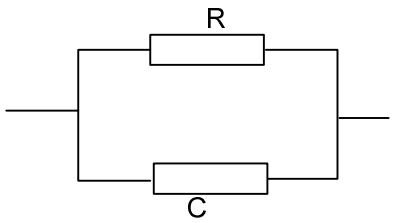

Figure 2.5 Modified electrical tissue model

Rewriting the above equation for Z in terms of R and S gives:

$$Z = \frac{RS/(R+S) + \left(R - RS(R+S)\right)}{\left(1 + \left(j_f / F_r\right)^{(1-\alpha)}\right)} \qquad (2.2)$$

where R is the extracellular resistance, S is the intracellular resistance , Fr is the dispersion frequency , α is the distribution constant and f is the frequency under investigation.

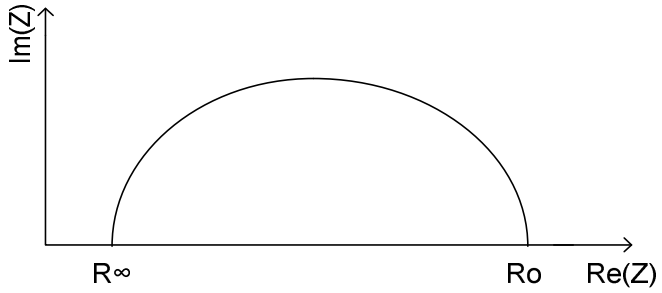

Figure 2.6 Cole-Cole plot of the real impedance

The Cole-Cole plot is a plot of the real part of impedance (resistance) versus the imaginary part of impedance (reactance). Constant cellular membrane behaviour illustrated in Figure 2.6 shows that the impedance of the cell is frequency dependent and will decrease in magnitude as the frequency increases. The imaginary part reaches a peak value when the frequency is the relaxation or characteristic frequency.

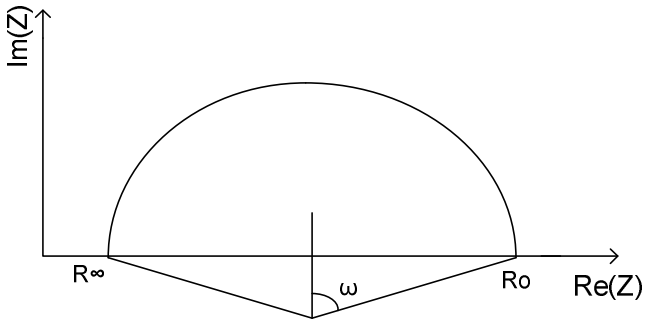

Figure 2.7 The Cole-Cole plot

A semi-circular arc in Figure 2.7 whose centre lies below the real axis illustrates the non-constant membrane characteristics of the cellular structure.

2.8 Summary

Electrical impedance mammography is based on the theory that there is a wide range of typical impedance values among various tissues. The multi-frequency response of tissue from several kHz up to several MHz can be constructed to characterise tissues and even the different states of the same tissue. Most of the development in EIT has occurred over the past twenty years and is summarised in this chapter. Electrical impedance mammography is one important application of the EIT technique to detect breast cancer at an early stage.

Chapter 3 Sussex MK4 EIM System

3.1 Introduction

The Biomedical Engineering group has been one of the leading research teams worldwide in this challenging and promising field for over 16 years since 1996. The group has been consistently making contributions to EIM, which has been its principal field of study. The group has been so successful, that work on EIM as a breast lesion detection modality has received approvals, both within the University and from the NHS, for a trial of the technique on healthy volunteers and symptomatic women respectively.

This chapter describes a general system introduction, system performance parameters, and measurement methods analyses. This section of the thesis also includes the system hardware modelling, explaining the analogue and digital acquisition hardware.

Table 3.1 Characteristics of impedance measurement system developed by the group.

System	Electrodes	Frequencies	Date
Mk1	4	Multi (100-4MHz)	1996
Mk 2	32	Multi (100-4MHz)	2000
Mk 3	32/64	16 (1-5MHz)	2002
Mk3	128	16(1-5MHz)	2004
Mk 4	85	Multi (1-5MHz)	2006

3.2 System Overview

The Sussex group has designed an 85 electrode multi frequency 3D EIM system (Henderson and Webster 1978, Barber and Brown 1984, Holder D S 2004) for breast examination.An AC current signal of not greater than 1mA (Béqo *et al* 2010) is applied on the electrodes over the range of 1 kHz-5MHz. Multichannel measurements are done

at 10 frequencies on both breasts. Each breast takes 4-5 minutes for the scan. A fully programmable planar array of electrodes is used by the system (Béqo *et al* 2010).

3.3 System Architecture

The operating parameters of the current fourth generation device are summarised in Table 3.2 below.

Table 3.2 Operating parameters of the Mark IV impedance measurement system developed by the group (Béqo *et al* 2010)

Channel	85
Bandwidth	100Hz-10MHz
Peak to peak current	0.1-1mA
Signal to noise ratio	≥60dB (1kHz-1MHz)
	≥40-46dB (1MHz – 5MHz)
Imaging frame rate	1 Frame/sec
Number of frequencies	10
Injection protocol	Four point
ADC	14-bit
Frequency selection	SW programmable
Electrode selection	SW programmable
Data storage	PC hard drive

The breast to be imaged extends through an opening into a plastic, cylindrical shaped scanner head filled with a body-temperature saline liquid with the patient lying comfortably face down on an examination table as depicted in Figure 3.1 (Béqo *et al* 2011). Fixed at the bottom of the saline filled cylinder is an 85 electrode planar array plate which is adjusted according to different breast sizes so that the breast comes in contact partially compressed. The plate is embedded in a sealed plastic housing that contains the driving circuit and the digitally controlled switching circuit.

Figure 3.1 Examination table

3.4 Image Reconstruction

The image reconstruction method used by the system is back projection. This method is based on differential voltage measurements. Change in impedance is mathematically calculated through the measured potentials on the breast, also known as the inverse problem (Calderon *et al* 1980) Figure 3.2. In the inverse problem, the measured potentials and applied currents are used to solve for the unknown impedance.

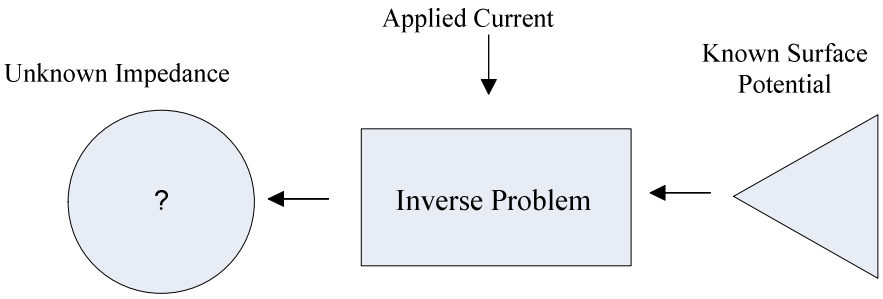

Figure 3.2 Inverse problem

3.5 System Performance

3.5.1 System signal-to-noise ratio (SNR)

The SNR describes the noise content in the signal. The SNR of MK4 EIM system is 40 dB from the front end of hardware before using signal processing methods to improve it to between 56-60dB.

3.5.2 Bandwidth

The -3dB point of the system with 0.6Vp-p input is at 1.55MHz.The bandwidth of the system is limited by the multiplexer capacitance.100pF of multiplexer capacitance produces a low pass filtering effect reducing the system bandwidth.

3.6 Medical safety

The application of an amount of current that is greater than a safe value to the patient is the most important aspect to be considered. Such currents may be due to systematic errors or may be due to leakage currents from the mains power supply according to EN60101-1 requirement .

Table 3.3 In-vivo maximum current limitation.

Frequency range (Hz)	Maximum current (μA)
<0.1	10
0.1-1k	100
1k-100k	1000 (frequency in kHz)
>100k	10000

The restriction of current below 0.1 Hz to only 10 μA is to limit the possible harm due to the electrolytic action of DC currents. The increase in allowable currents above 1kHz

is due to the reduction in biological sensitivity at higher frequencies (Lionheart *et al* 2001).

3.6.1 Mains supply isolation

The mains supply is of low frequency and is relatively dangerous in comparison with the signals applied by the EIT. Safety in the Mk4 System is provided by isolating the equipment power supply from the mains supply. During the scan, the equipment is powered by using a 12V DC supply.

3.7 System Hardware Model

The hardware of the Sussex Mk4 system is summarised in Figure 3.3 and meets the overall systematic specification given in Table 3.4.

A 1V voltage signal applied by the National Instruments (NI) chassis to a voltage to current converter will generate a 1mA constant current. The current is injected into the electrodes to measure the subject impedance.

Table 3.4 Hardware specifications of Mk4 EIM system

Applied current	0.1-1mA
Electrodes	85 fully programmable electrodes
Measured potential	Real and imaginary
Dynamic range	1.5-2.2
Bandwidth	100kHz-10MHz
Signal to Noise ratio	1kHz-1MHz > 60dB
	1MHz-5MHz > 46dB

As shown in the block diagram of Figure 3.3, the Sussex Mk4 system consists of three main parts namely: a host PC; digital circuitry and analogue circuitry.

3.7.1 Host PC

Firstly, the host PC defines measurement parameters and downloads data to the NI chassis with a specific format. After measurement the data processing and image reconstruction are completed by the PC.

3.7.2 Digital part (NI-chassis)

The NI chassis controls the signal generation, address multiplexers and demodulates the measured signals.

The chassis with a number of dedicated PXI modules is controlled by software. The PXI module comes with driver installation software and an Application Programming Interface (API) which is called and controlled by LabVIEW™ (Béqo *et al* 2010).

3.7.3 Analogue part

The analogue system consists of voltage to current converter, analogue multiplexers and amplification.

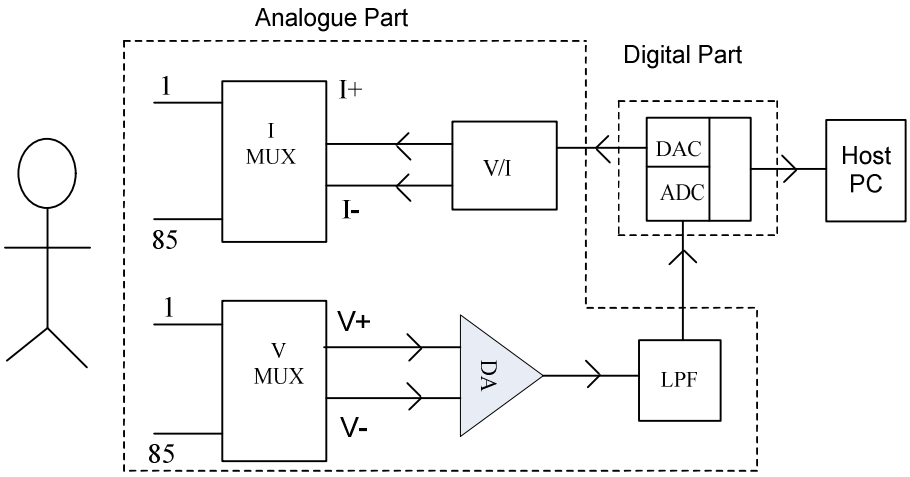

Figure 3.3 Block diagram of EIM acquisition system

The working of the Mk4 system is described as follows:

1. A NI based programmable digital waveform generator generates a sine wave with frequency range up to 5MHz.
2. A voltage controlled current source forms a current source (V-I). The multi-frequency voltage signals from the function generator are fed to the V-I to generate the same magnitude positive, I^+, and negative, I^- , currents.
3. The analogue multiplexers are used to switch (I^+) and (I^-) between a different pair of electrodes whilst measuring potentials from the pair of electrodes. All designated pairs of current and voltage electrode addresses are controlled via a digital NI controller.

3.8 Current injection protocol

85 electrodes are arranged in an hexagonal pattern as shown in Figure 3.4 and are positioned equal distances of 17mm from each other. The circular diameter of each electrode, arranged in a planar array configuration, is 2mm.122 different injection drive patterns are used for 1416 total measurements. Each drive requires a maximum of 12 voltage measurements per frame. The switching of the electrodes for each frame is driven by a multiplexing arrangement (Sze *et al* 2011).

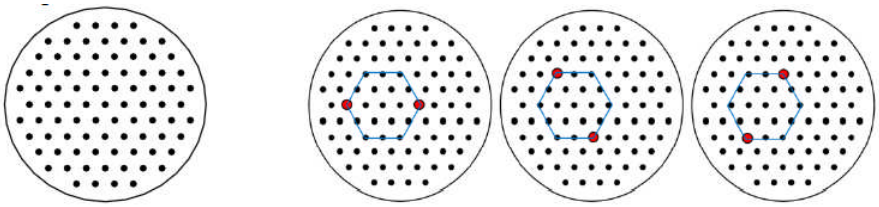

(a) (b) (c)

Figure 3.4 85 electrodes in an hexagonal arrangement (a) (b) and (c). Three rotations of drive electrodes (in red) for a local region (blue hexagon outline) (Sze *et al* 2011).

3.9 Voltage Measurement Protocol

In order to avoid the effect of electrode impedance during measurement, four electrode methods are used. Figure 3.5 (a) and (b) showing the four point equivalent measurement methods.

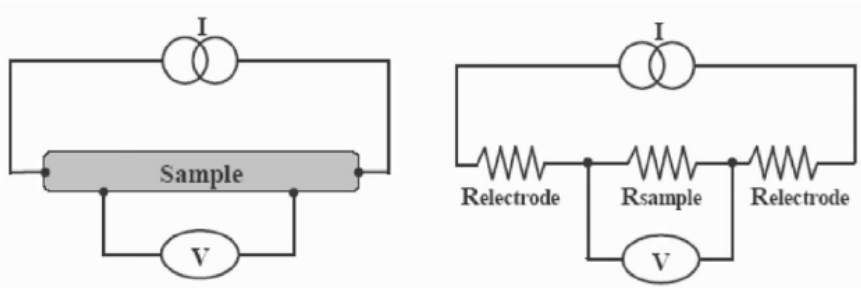

(a) (b)

Figure 3.5 (a) Block diagram representation (b) Four electrode equivalent circuit diagram.

3.10 EIM Acquisition Analogue Part

3.10.1 Voltage to current converter

Current is applied to two electrodes using a serial injection protocol (McEwan *et al* 2007), measuring the developed potential on the different pairs of electrode through software. Current injection is done by the current source with available output frequencies that are continuously variable over a wide bandwidth.

Two single ended identical current sources with a 180° phase shift are used for the injection of current. Sine wave current injection is chosen because for a 2-D circular object, trigonometric current patterns would provide 30 times better distinguishing ability (Zou and Guo 2003).

With a 180° phase shift, one electrode becomes the source and the other is the sink for a balanced current source. Current source configurations as single ended and electrode injection are shown Figure 3.6.

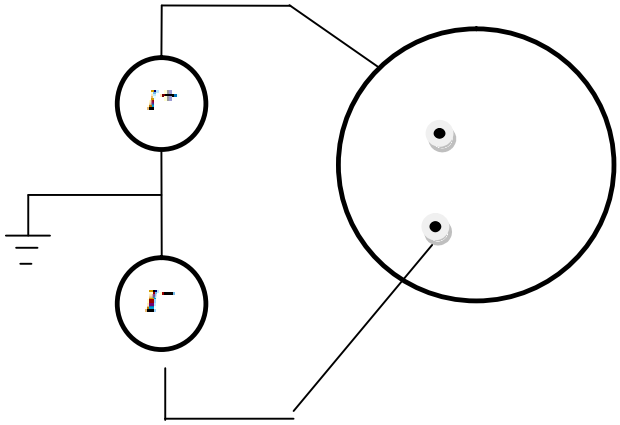

Figure 3.6 Injection current on Electrodes E1 and E2 through dual single ended current sources.

The enhanced Howland method is used for the 100Ω-40kΩ load impedance over a 1 kHz - 5 MHz frequency range. Input to the V/I stage is from a 14 bit function generator of the NI series.

3.10.2 Analogue multiplexer

Currents are switched between the pairs of electrodes through an analogue multiplexer. Eight analogue multiplexers have a total of 8 x 12 = 96 channels in the injection system, out of which 85 channels are used.

Using the control software, any two electrodes apply current to the breast while any other two detect the developed potential difference. Each electrode can be either configured for current injection or voltage measurements. At a time one channel can have one output only, either I^+ or I^- . So from one analogue multiplexer there are six I^+ and six I^-. The MUX input and output concept is explained with the aid of Figure 3.6(a) ,(b) and (c). The current source and analogue multiplexer configurations in block diagram form are shown in Figure 3.7 and Figure 3.8 shows the layout of the multiplexer switch in terms of ON resistance, R_{ON}, and switch ON capacitance, C_{ON}.

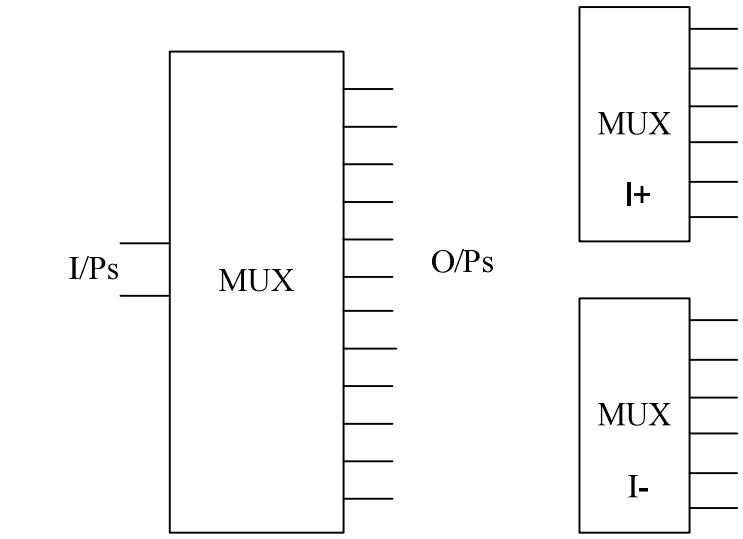

a) b)

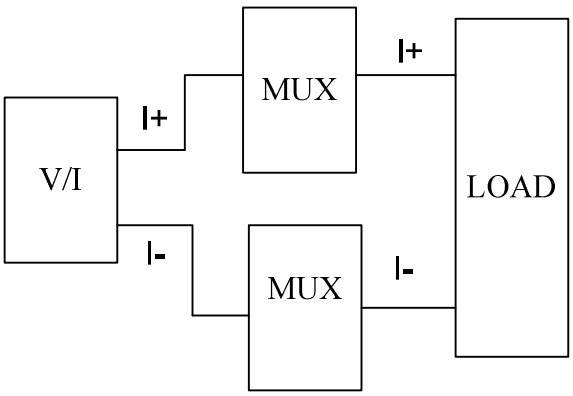

c)

Figure 3.6 (a) and (b) MUX concept (c) Two single ended current sources and the MUX concept

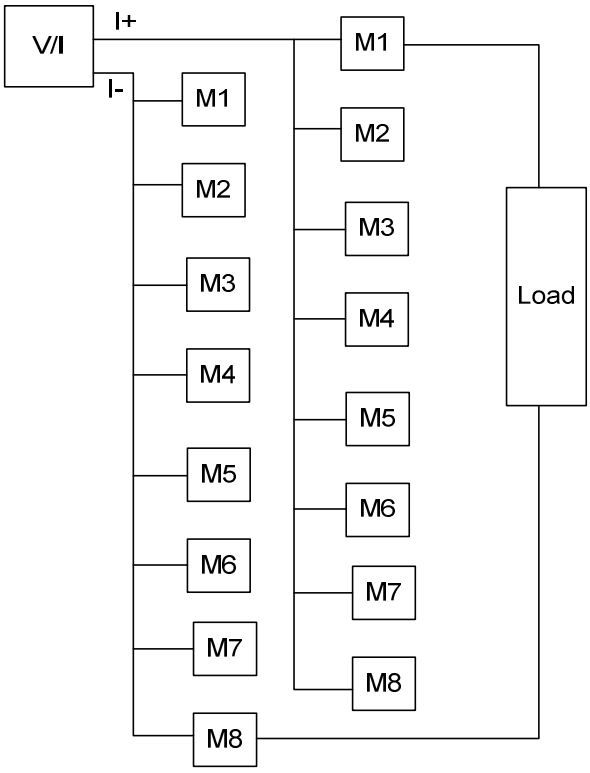

Figure 3.7 Current sources and multiplexers block diagram layout.

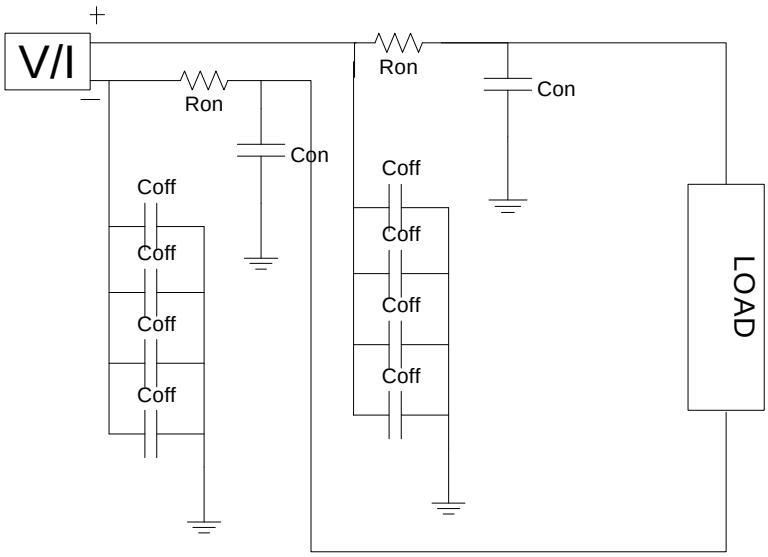

Figure 3.8 Current sources and multiplexers layout in terms of capacitance.

The bandwidth of the current system is limited by the current source and multiplexer layout shown in Figure 3.8. It has been suggested that by applying signals above 1 MHz an increase in the diagnostic value may be achieved (Ryan *et al* 2008).

The current MK4 EIM injection stage configuration comprises two single ended current sources which are used for the polar sine wave injection. Transmitting analogue multiplexers with input capacitance (C_{ON} and C_{OFF}) as shown in Figure 3.8, introduce a 100pf low pass effect, limiting the bandwidth to 1.5 MHz.

3.11 EIM Acquisition: Digital Part

The PXI chassis implements all functions of the digital part i.e. the sine wave generator, digital control signal, multiplexer control and digital demodulation (Béqo *et al* 2010).

3.11.1 Sine wave generator

The PXI board generates a sine voltage for the DAC. The following parameters are considered for sine wave generation.

1) Frequency of the sine wave
2) Amplitude and amplitude stability of the sine wave
3) Phase and phase shift of the sine wave
4) Sampling frequency and DAC resolution

The frequency of the sine wave is specified from 1 kHz to 5 MHz. The amplitude of the sine wave is set to 2 V_{p-p} and is equally divided into 4096 samples to get a small and precise threshold value. The phase of the sine wave can be set to any phase at the start of the DAS.0° phase is set in the Mk4 EIM system. The resolution is 12-bits.

The digitizer, function generator and EIM circuit block diagram configuration is described in Figure 3.9.

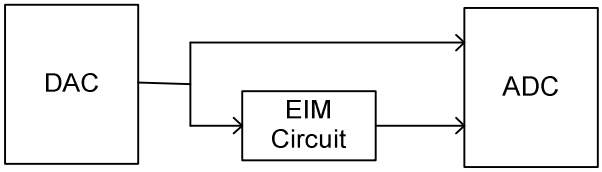

Figure 3.9 DAC and ADC configuration with EIM circuit

3.11.2 Digital demodulation

Due to the frequency range used, the developed potentials are digitized via a NI digitizer for streaming to the computer. The block diagram for digital demodulation is shown in Figure 3.10.

A 12 bit digitizer with a sampling frequency of 100M samples/sec is used for this purpose.

For EIT signal demodulation, a high precision ADC is required. Thus demodulation of the measured signal is done by a 14 bit NI digitizer, sampling at 100M samples/sec. The 14 bit digitizer has 16384 quantised levels with a $2V_{p-p}$ measurement range and has a voltage resolution of 0.122mV /step.

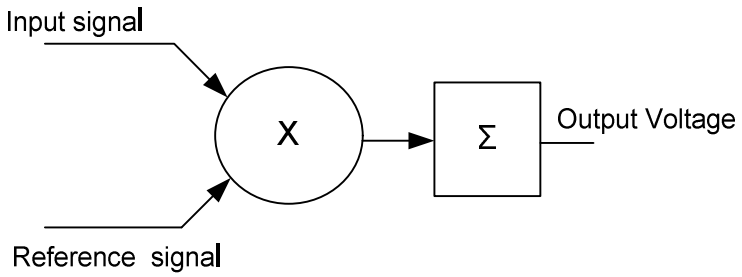

Figure 3.10 Block diagram of the digital demodulator

In our system, the signal is sampled at a rate much higher than the Nyquist frequency and then digitally filtered to limit it to the signal bandwidth.

3.12 Summary

This section gives an overview of the Mk4 system measurement protocols and system performance. A flexible hardware system suitable for wide frequency ranges has been implemented with the combination of digital and analogue parts.

The signal generator (V-I) and multiplexers are the important parts as they affect directly the performance of the acquisition system.

Chapter 4 Contributing sources of artefacts limiting system performance and image quality of Sussex planar array EIM system

4.1 Introduction

An analysis of possible factors affecting the image quality, image reconstruction and system performance of the MK 4 Planar Array EIM system is presented. The main reason for this study is to identify the major contributing sources of artefacts limiting the system performance and image quality in the clinic.

Possible factors affecting the system are categorised and studied as: artefacts introduced by the patients while scanning; internal and externally introduced frequency dependent noise;, contact impedance and hardware limitations degrading system performance due to stray capacitance and cable connections.

4.2 Purpose of this study

The system performance and source of data quality limiting factors are discussed in detail to understand their effect on the existing Mk4 system performance and their impact on the reconstructed conductivity images.

Three main distinct measures compromised are signal to noise ratio (SNR),roll-off and artefacts. Potential errors in the Sussex Planar Array EIM system are classified into three broad categories on the basis of noise, external and systematic (non-linearity errors caused by the hardware and image reconstruction, sensors, control etc.) errors as summarised in Figure 4.1.

1) External errors
    a. EM interference
    b. Patient artefacts (dry skin, movement, patient-electrode contact etc.)
2) Systematic errors affecting system performance

a. Bandwidth limitation due to analogue multiplexer and current source configuration.
b. Current source error 1: Output current.
c. Current source error 2: Output impedance.
d. Common mode voltage.
e. EIM sensor system error (due to electrodes and acrylic plate configuration).

3) Noise:
   a. Predictable noise (includes frequency dependent noise introduced by the electronic system e.g. colour or white noise etc).
   b. Unpredictable noise (includes frequency dependent noise introduced by the electronic system e.g. colour or white noise etc).

In this chapter the possible errors and artefacts are structured and characterised in detail.

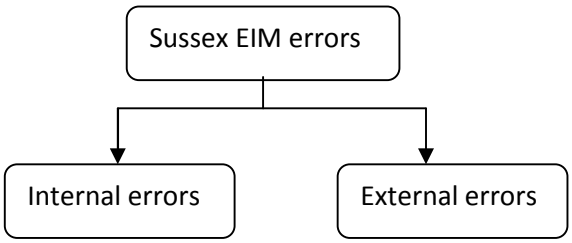

Figure 4.1 Block diagram error representation of Sussex MK4 EIM System

4.3 Possible external sources of errors affecting image quality and system performance

Artefacts introduced by the patients and the patient-electrode interface are the main challenges faced by EIT technology. These artefacts not only affect the repeatability and accuracy of the system performance but also the reconstructed image quality (Hua *et al* 1993, Kolehmainen *et al* 1997, Nissinen *et al* 2009).

Though the wet electrode (Wang *et al* 2010) implemented by the Sussex EIM system eliminates the direct patient-electrode interface using a dielectric medium, nevertheless unexpected abnormal threshold levels were noticed during the clinical data analysis. These undesired threshold levels were noticed between the acquired measurement frames responsible for the artefacts in the reconstructed conductivity images (Hua *et al*

1993). Upon further analysis it was discovered that these unwanted levels varied with the subject (Wang *et al* 2010). Infinite impedance due to electrode blockage is a factor in the occurrence of these abnormal measurements. Several unexpected artefacts discussed in this section are categorized keeping in view the entire scanning procedure and analysis of the data. These unexpected changes of the scanning subject artefacts are classified below in Figure 4.2.

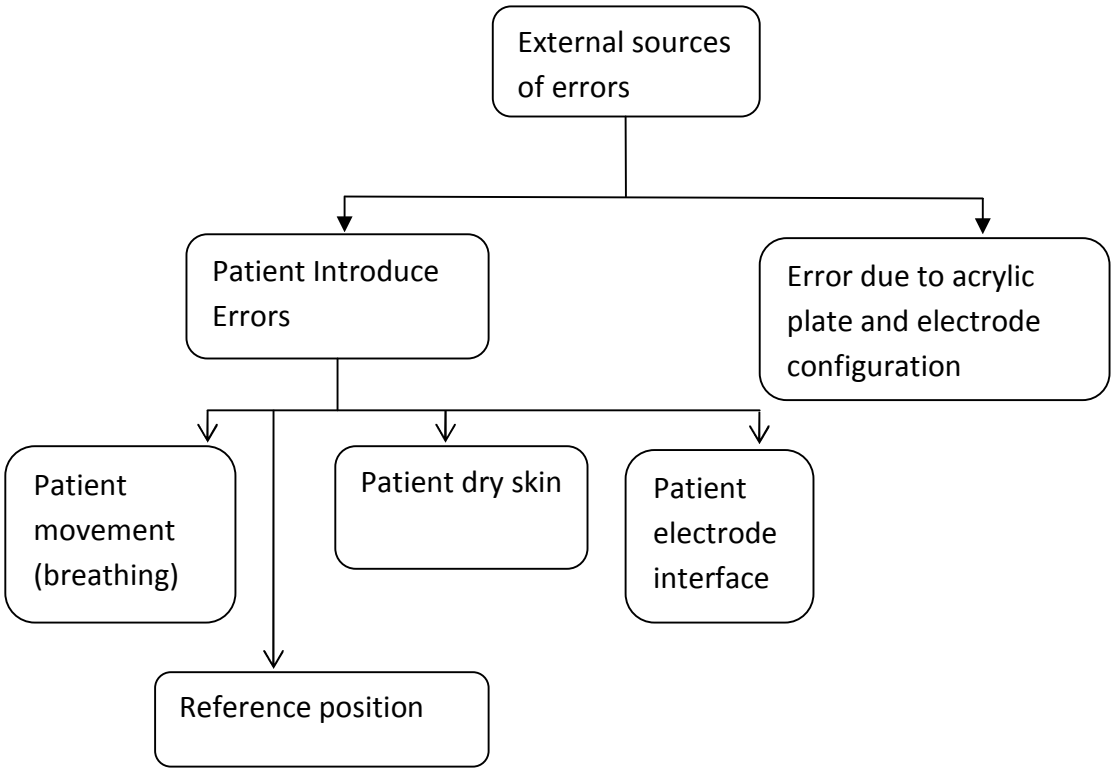

Figure 4.2 Block diagram representation of possible external sources of errors

4.3.1 Patient's dry skin

It has been observed that dry skin immersed in saline produces bubbles on the skin. The air remained trapped in small bubbles in the fine hair of the skin. These trapped air bubbles introduce artefacts in the measurement frame causing the acquired voltage to deviate from normal levels.

4.3.2 Patient moving artefacts

Patient movement and breathing during the measurement frames effects the results. The patient needs to be as still as possible holding their breath for 90 sec. Breathing effect limitation can be overcome by reducing the scan time of the system. The scanning time depends on several factors including the acquisition format used by the controlling (or acquiring) software and should be the same as that of the analogue-to-digital converter (digitizer). Also, the analogue multiplexer should have minimum ON and OFF switching times.

4.3.3 Patient -electrode contact

During the scanning, it was observed that the weight and the skin of the subject displaces the saline from the 2mm deep electrode cavity shown in Figure 4.3 (Wang *et al* 2010) removing the contact medium. This no contact medium condition will result in infinite impedance between the electrode and the skin causing the acquired voltage levels to deviate from their normal values.

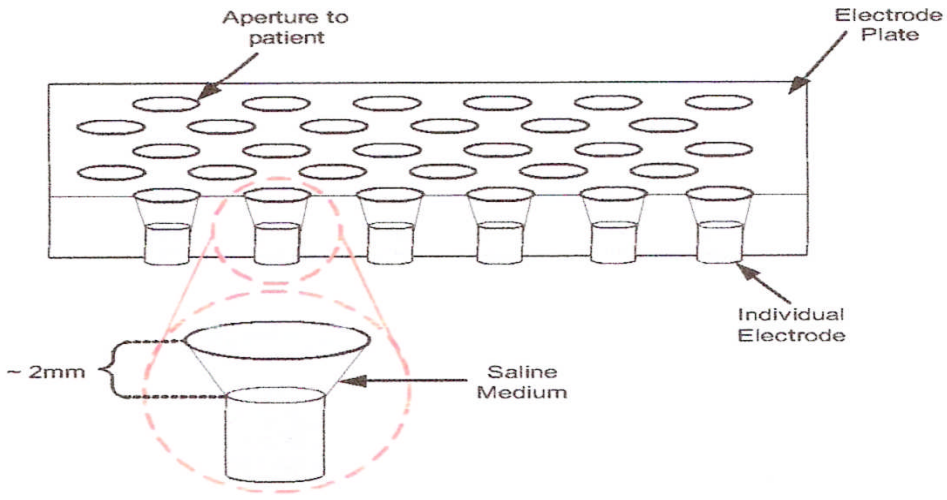

Figure 4.3 Sussex Mk4 EIM planar electrode array showing the wet electrode interface (Wang *et al* 2010).

4.4 Systematic errors affecting system performance

System performance errors can be categorised as indicated in Figure 4.4.

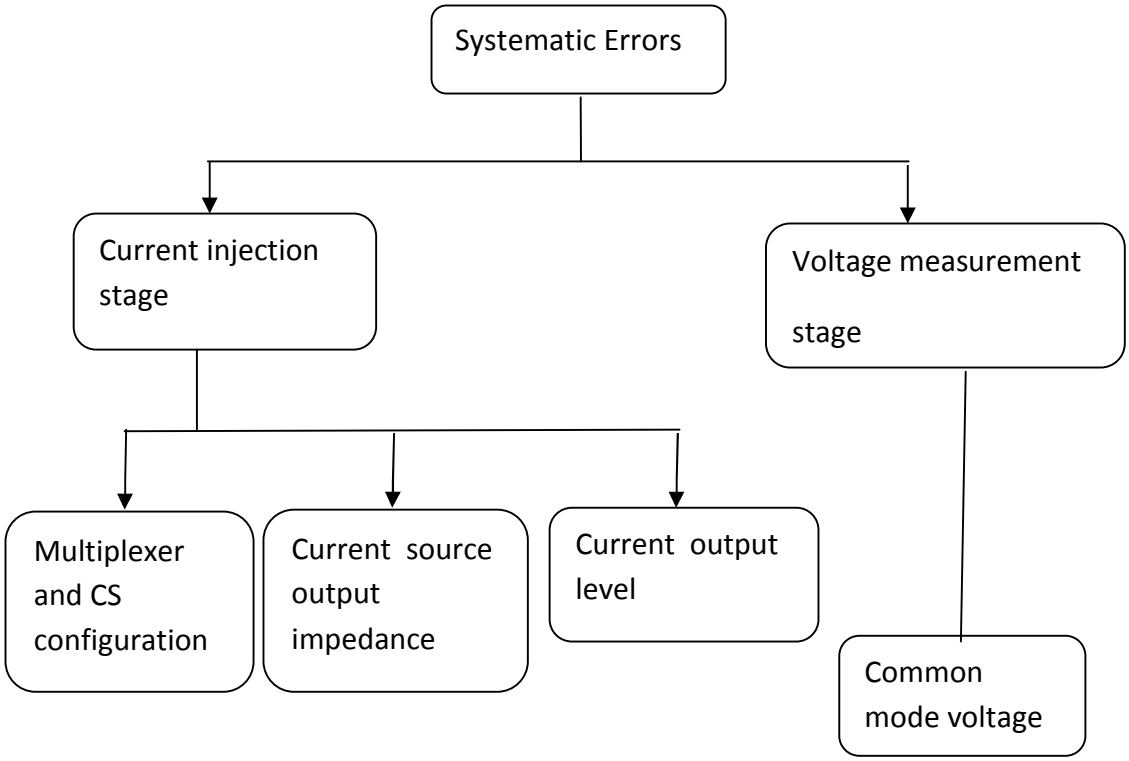

Figure 4.4 Block diagram representation of Sussex MK4 EIM systematic errors

4.4.1 Bandwidth limitation due to analogue multiplexer and current source configuration

The bandwidth of the current system is limited by the current source and multiplexer configuration, shown in layout form in Figure 4.5. It has been suggested that by applying signals above 1 MHz the diagnostic value may be increased (Ryan *et al* 2008).

The current MK4 EIM injection stage configuration comprises of two single ended current sources which are used for the polar sine wave injection. The transmitting analogue multiplexers' input capacitances (C_{ON} and C_{OFF}) shown in Figure 4.6 introduce a 100pF low pass effect, limiting the bandwidth to 1.5 MHz.

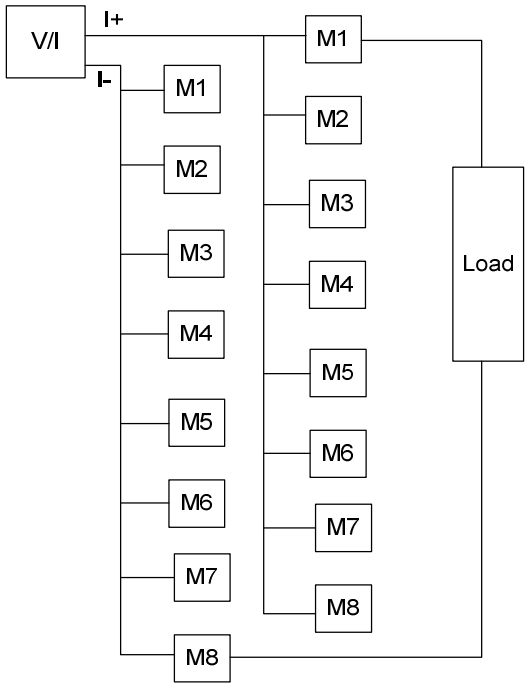

Figure 4.5 Current source and multiplexers block diagram layout.

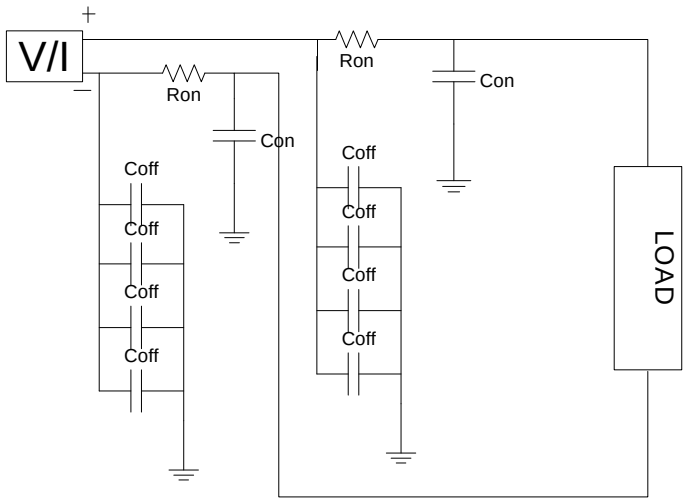

Figure 4.6 Current sources and multiplexer layout in terms of C_{ON}, C_{OFF} and R_{ON}.

4.4.2 Current Output

The total amount of the drive current must be limited within the range regulated by Medical Electrical Safety Regulations in order to ensure the safety of human beings. The amount of current that can be injected to the human body can be 100μA x f (Xuetao

et al 2006,A McEwan *et al* 2007). The Sussex Mk 4 system uses $0.6\ mA_{p-p}$ of injection current for scanning different subject volumes and densities. The embedded electrode plate adjusts accordingly to different depths for different breast volumes so that the breast comes in contact partially compressed. Injecting $0.6\ mA_{p-p}$ for the higher depths would record lower voltage levels with higher noise levels.

Wang et al 2010 has given the rational of the acquired single electrode measurement with respect to different depths, shown in Figure 4.7. It is evident from Figure 4.7 that the acquired electrode voltages are high enough to dominate the noise introduced by the external sources and the electronic circuitry at the lower depths.

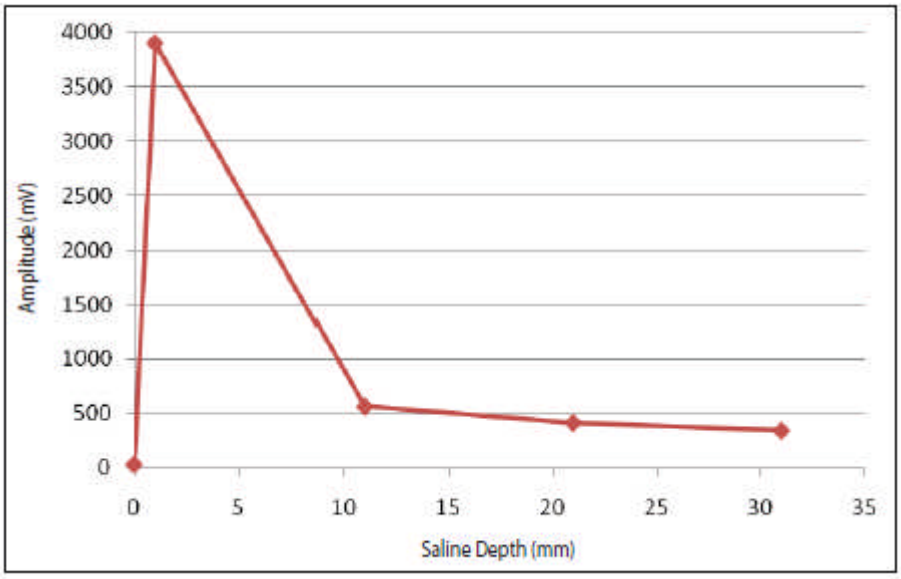

Figure 4.7 Measured values of single electrode combination against depth with 0.5mS/cm saline (Wang *et al* 2010)

The injecting current can be increased to $2.8\ mA_{p-p}$ in order to achieve greater boundary voltages and SNR (Xuetao *et al* 2006). Also, it is suggested to use 0.3mS/cm for the scanning of patients instead of 0.5mS/cm in order to have higher boundary voltages and SNR.

For different depths, various contact media of different conductivities can be used to obtain maximum acquired voltages. Figure 4.8 shows the 12 measurement frame

acquired potential at a standard 45mm depth with 0.3mS/cm, 0.5mS/cm and 0.7 mS/cm at room temperature. It is clear from these results that using the 0.3mS/cm dielectric medium will result in a better electric potential acquired by the subject as compared to 0.5mS/cm and 0.7mS/cm. In case of 0.3mS/cm, breast will have higher impedance hence acquiring a higher potential drop.

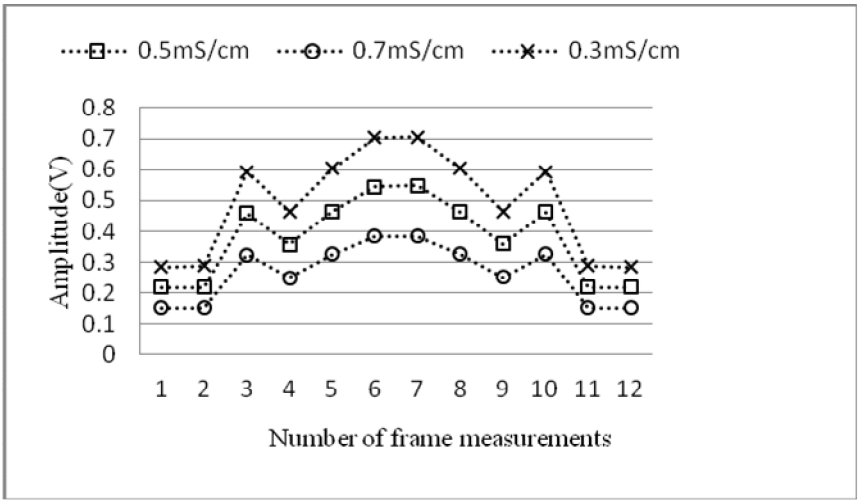

Figure 4.8 Single frame measurements with 0.3mS/cm,0.5mS/cm and 0.7mS/cm.

4.4.3 Current source output impedance

Current sources designed for EIT applications (Cook *et al* 1994, Ross *et al* 2003, Cherepenin *et al* 2001, Hartov *et al* 2000) are desired to have the applied current remain unchanged for a wide range of load impedances and so it is necessary to have a current source with ideally infinite output impedance of the bandwidth of use. In practice, high output impedance is difficult to obtain due to stray capacitance shunting the output impedance as shown in Figure 4.8.

4.4.4. Common mode voltage

An instrumentation amplifier is used to measure differential voltages between the two electrodes. High impedance is desired to prevent the sinking of current through the amplifier causing common voltages appearing on the measuring electrodes. A good

common mode rejection ratio (CMRR) is an amplifier requirement. While the drive signal is usually a constant current, the measured differential voltage has significant dynamic range. A fixed gain voltage amplifier will struggle to maintain a good SNR and hence an automatic multiple gain control amplifier is required. In the Sussex EIM system, a differential receiver amplifier used a high CMRR of 70dB at 10 MHz with a user adjustable gain.

A high-pass filter with an existing cut-off frequency of almost 10Hz is shown in Figure 4.9.In order to avoid common 50Hz and 100 Hz interference, the cut-off frequency of each high-pass filter should be greater than 200Hz .

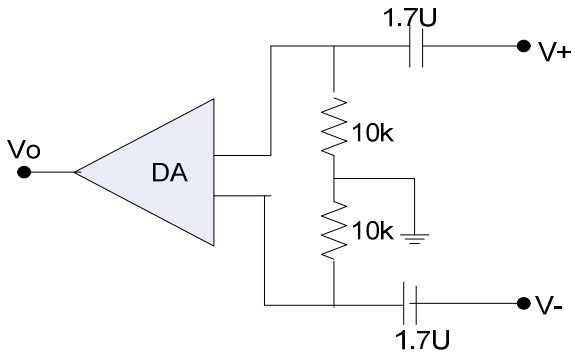

Figure 4.9 Current V3 system configuration

4.4.5 EIM sensor system error (error due to acrylic plate and electrodes configuration)

The Sussex data acquisition system is fixed at the bottom of the cylinder in a sealed plastic housing that contains the driving circuit and the digitally controlled switching circuit. This effective closed configuration of the acquisition circuitry and the stainless steel electrodes is achieved by using the pins instead of wires. Shown below in Figure 4.10 is a block diagram representation of the circuit and the electrode configuration. Using pins has not only reduced the stray capacitance effect at higher frequencies but also has eliminated the effect of noise introduced due to the wires' resistance and unreliable cable connections due to patient movements.

It is very important to configure the electrodes in the acrylic plate with great precision to avoid unexpected artefacts due to any micro gaps present. These micro gaps will result in bubble formation due to the air pockets contained within these micro gaps.

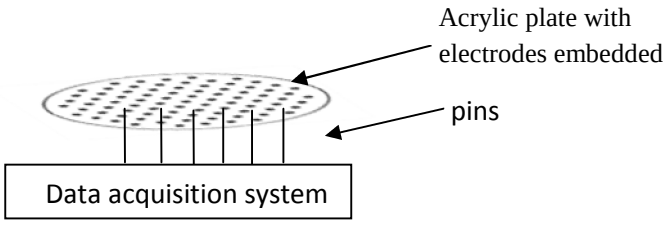

Figure 4.10 Block diagram representation of acrylic plate with electrodes and data acquisition system.

4.5 Noise

Repeatable and unpredictable noise sources are described below that might affect the signal quality and system performance.

4.5.1 Predictable sources of noise

Repeatable noise in the system remains at the same level irrespective of the input (Xuetao *at al* 2006). They possibly could cause frequency dependent DC offset and phase shifts within the measured signal and act as a low pass filter. This low pass effect will change the magnitude of the received signal at different frequencies. As image reconstruction is based on the voltages measured from the electrodes, the smaller the voltages are, the more influence small amounts of noise will have. electronic noise in the system is easily filtered out through software calibration.

Major contributing sources of repeatable systematic errors and noise in the Sussex EIM system might be white noise due to the electronic components used, stray capacitance due to the PCB tracks and any imperfect cable connections. Noise due to internal electronic circuitry is repeatable and can be filtered out using software calibration.

4.5.2 Unpredictable source of external interference

As named, these noise sources are random and are caused by all unpredictable sources. They cannot be predicted and repeated. External noise in the MK4a EIM system includes artefacts caused by patient movement and room wall banging due to close proximity of X-Ray CT scanning. This results in a sudden change to the detected measurement. Most of the external sources are random and difficult to filter out due to the wide frequency bandwidth.

4.6 Discussion

In this chapter three major data quality and system performance issues are discussed in detail which includes the noise, external (patient introduced) and systematic sources of errors. In order to have high signal to noise ratio (SNR), high gain, low noise front end design with high quality chips can be used.

Patient introduced external sources of errors discussed above are analysed in detail in Chapter 5 and ways to mitigate these errors are discussed in Chapter 6.

Systematic errors can be minimised by overcoming the bandwidth limitation, current output and current source output impedance discussed in Chapter 7.

4.7 Summary

In this chapter the three major data quality and system performance issues are discussed in detail which includes the noise, external (patient introduced) and systematic sources of errors. Front end circuitry is proposed to improve SNR and proposals to reduce systematic errors are discussed later in this research.

Chapter 5 Investigation of undesired voltage threshold levels on an EIT planar array system for in-vivo breast cancer

5.1 Introduction

Impedance-based mammography techniques have suffered from relative inaccuracy due to practical problems with electrode-skin contact (Boone *et al* 1996, Kolehmainen *et al* 1997,Nissinen *et al* 2009, Tunstall *et al* 1997,Hua *at al* 1993, Wang *et al* 2007, Wang *et al* 2010). The Sussex EIM system uses a 'wet' electrode (Wang *et al* 2010) shown in Figure 5.1, which allows indirect contact between the skin and electrodes through a dielectric medium, helping in the reduction of contact impedance. Electrode blocking introduces artefacts in the reconstructed conductivity images with a greater effect in absolute imaging, as the forward solution depends on the electrode skin contact impedance (McEwan *et al* 2007, Boone *et al* 1996).

While analysing the acquired data it has been noticed that at certain electrode combinations the acquired signal response is saturated and/or zero. Complete electrode blockage results in dead or saturated signals on the particular electrode combination.
This study includes a number of possible factors and their solutions responsible for unwanted affects, a comprehensive study and analysis of what ratio of electrode blockage can affect the acquired raw data, so compromising the reconstruction that follows and techniques for fast detection of any such occurrences.

The errors discussed in this chapter are

a. Patient introduced errors.
b. Systematic errors.
c. EIM sensor system error (hardware configuration error).

5.2 Purpose of this Study

While analysing the acquired data it has been noticed that with certain electrode combinations the acquired signal response is saturated and/or zero. Complete electrode blockage results in dead or saturated signals on the particular electrode combination.

This chapter describes a number of possible factors responsible for unwanted affects and their solutions. A comprehensive study and analysis is carried out to what ratio of electrode blockage can affect the acquired raw data and how this compromises reconstruction. Techniques for fast detection of any such occurrences are finally described.

5.3 Possible factors causing saline displacement

The patient electrode interface (Wang *et al* 2010, Beqo *et al* 2011) is the important challenging aspect to be investigated in detail. Undesired threshold voltage levels between the acquired measurement frames will be the cause of artefacts in the reconstructed conductivity images (Hua *et al* 1993). Infinite impedance due to electrode blockage is a factor in the occurrence of these abnormal measurements. The infinite impedance effect is more marked in absolute imaging, as the forward solution is strongly reliant on the electrode-skin contact impedances (Kolehmainen *et al* 1997, Nissinen *et al* 2009).

Possible factors strengthening infinite impedance occurrence are discussed below.

5.3.1 Patient introduced errors

Patient’s dry skin: It has been observed that dry skin immersed in saline produces bubbles on the skin. It was observed that air remained trapped in small bubbles in the fine hair of the skin.

Skin and weight: Electrode plate partially compressed for the scanning purpose with the breast causes saline to displace from the 2mm electrode cavity (Wang *et al* 2010) shown in Figure 5.1. Experiments carried out on volunteers for the Mk4 System showed saturated measurements along with very low or zero acquired data. This condition varied with the subject making it obvious that it is not something that has to do with the systematic error. A possible reason for these unwanted acquired voltage levels is due to the weight of the breast removing the contact medium.

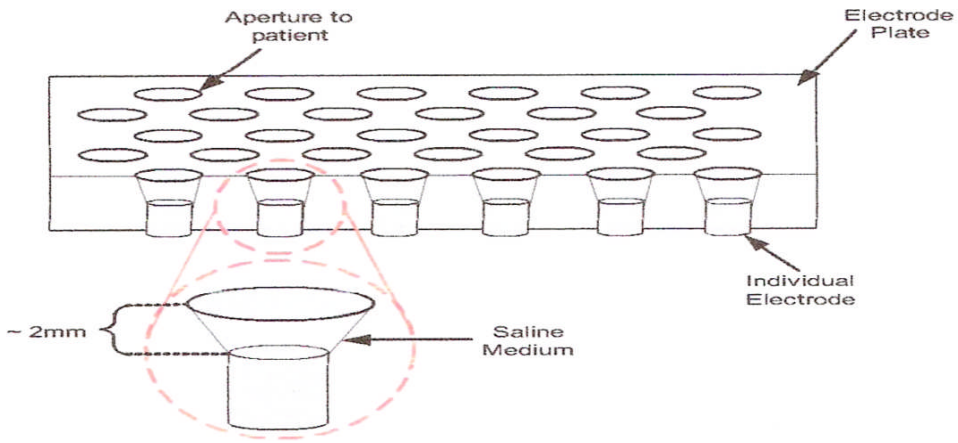

Figure 5.1 Sussex Mk4 wet patient-electrode interface with "non-contact" design (Wang *et al* 2010)

5.3.2 Systematic errors

Electrolysis: Electronic circuits connected to electrodes can possibly cause frequency dependent DC offset resulting in bubble generation on the immersed electrodes as shown in Figure 5.2 below. This DC offset can be generated during switching of the electrodes, or by electrodes not used for injection and acquiring at that point etc. As the DC signal passes through and between the electrodes, the saline solution splits into hydrogen and chlorine gas, which collects as very tiny bubbles around and on the electrode.

There are a number of considerations to reduce any DC offset by careful design in the front-end electronics link to the electrodes. However, the DC offset will remain at some level between the electrodes.

These generated bubbles cover some ratio of the electrode area; the extent of this, that affects the acquired voltages, has been determined and is discussed in this chapter.

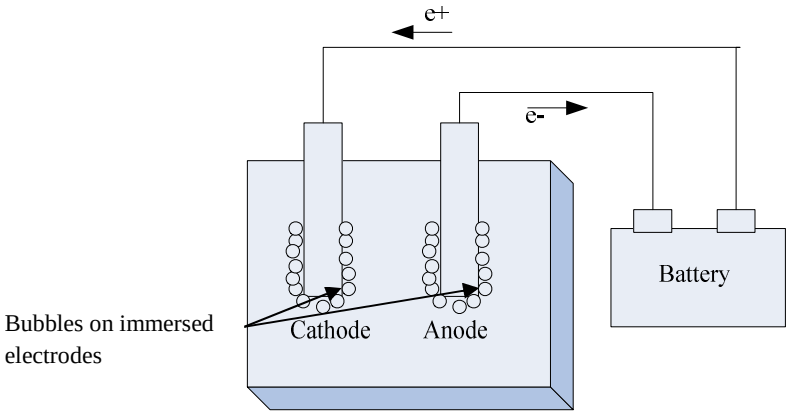

Figure 5.2 Bubble generation due to DC offset

5.3.3. EIM Sensor system error

Micro gap between the electrodes and the plate: While investigating the possibilities of bubble generation, it is observed that the bubbles are generated if the `dry` scanner head is filled with dielectric medium for scanning the volunteers. These bubbles keep on growing because of the micro gaps between the electrodes and the acrylic plate as shown in Figure 5.3. Different sizes of the bubbles generated on the electrodes will at some ratio block the electrode so affecting the acquired voltages.

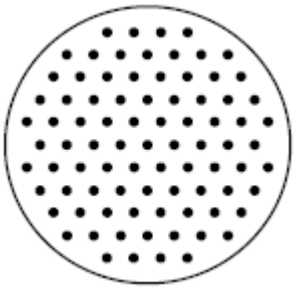

Figure 5.3 Plain acrylic plate with electrodes

5.4 Blocked electrode effect on the acquired signal

The acquired signal when analysed through offline analysis shows saturations or dead channels in the presence of bubbles or electrode blockage as indicated in Figure 5.4.

2D impedance representations of dead and saturated channels are shown in Figure 5.5 (a) & (b) indicating the saturated channel in a bright red colour.

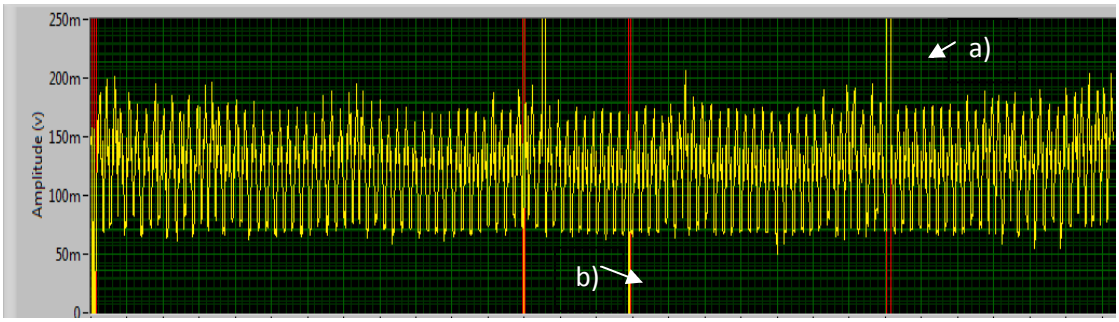

Figure 5.4 Dead and saturated electrodes combination: a) Saturated b) Dead

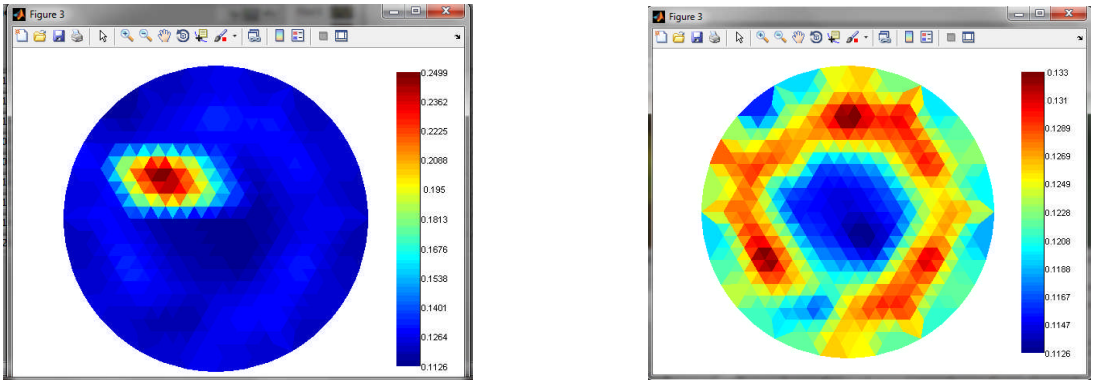

(a) (b)

Figure 5. 5 2D Impedance image indicating saturated (a) at the 10 o'clock position and (b) dead channels in a ring in red.

5.5 Different bubble sizes and their effect on the acquired signal

This section investigates at what ratio of the 2mm electrode blockage unwanted threshold voltage levels occur that are responsible for artefacts appearing in the reconstructed conductivity images (Sze *at al* 2010) . For this finding and analysis, different sizes of bubbles were artificially introduced on driving and receiving electrodes to provide a forced blocking as shown in Figure 5.6. Bubbles covering 1/8, 1/4, 1/2 and full electrode diameter were artificially introduced using a syringe as shown in Figure 5.7. This experiment was carried out by filling the scanner head with saline of 0.5mS/cm conductivity at room temperature.

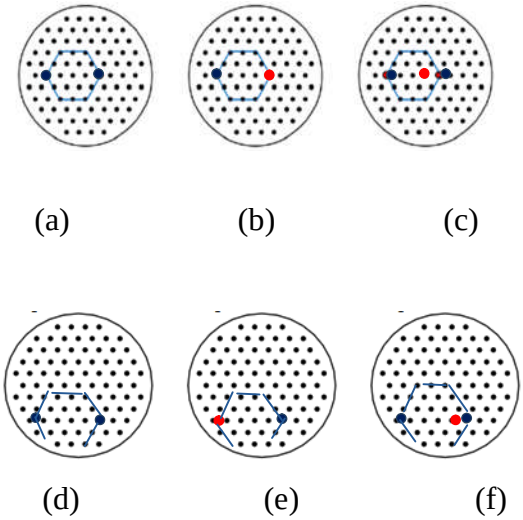

Figure 5.6 (a) Symmetrical frame drive-electrodes for a maximum 12 measurements (blue hexagon) (b) Symmetrical frame drive- fully blocked receiving electrode (in red) (c) Symmetrical frame drive -fully blocked driving electrode (in red) (d) Non-Symmetrical frame drive-electrodes for a maximum 12 measurements (blue hexagon) (e) Non-Symmetrical frame drive- fully blocked receiving electrode (in red) (f) Symmetrical frame drive -fully blocked driving electrode (in red).

Figure 5.7 Bubble generation method by using a syringe

5.6 Discussion

Analysis of the results is carried out in two stages; first comparison is done with the threshold levels at different acquisition frequencies (50kHz and 500kHz) with the electrodes blocked to certain defined ratios (Bilal *et al* 2011).

Second, a set of analyses is carried out by the comparison of different threshold levels caused different ratios of electrode diameter blockage at 50kHz and 500kHz.
Measurement frames considered for the analysis have either 10 or 12 number of points. 10 point measurement frames are known as non-symmetrical, whereas the 12 measurement frames are defined as symmetrical.

A single drive symmetrical frame shown in Figure 5. 6 a), b) and c) indicates 12 voltage measurements and Figure 5.6 d), e) and f) show non-symmetrical 10 voltage measurement frames.

5.6.1 Symmetrical driving electrodes

Table 5.1 Comparative analysis of SNR and voltage with different bubble sizes at 50kHz.

Bubble size	SNR_{max} (dB)	SNR_{min} (dB)	V_{max} (mV)	V_{min} (mV)
1/8	39.49	32.98	368	174
1/4	40.47	35.33	345	203
1/2	40.89	31.29	387	180
Full	11	6	12	4
No bubble	40.34	33.71	383	183

Table 5.2 Comparative analysis of SNR and voltage with different bubble sizes at 500 kHz

Bubble size	SNR_{max} (dB)	SNR_{min} (dB)	V_{max} (mV)	V_{min} (mV)
1/8	27.84	19.39	98	42
1/4	27.84	19.38	99	42
1/2	30.12	22.74	112	51
Full	10.42	4.67	10	4
No bubble	29.27	21.82	115	53

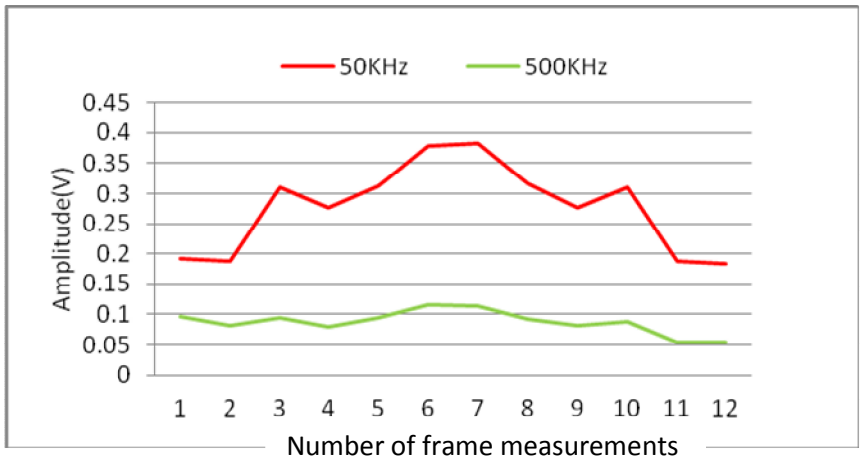

(a)

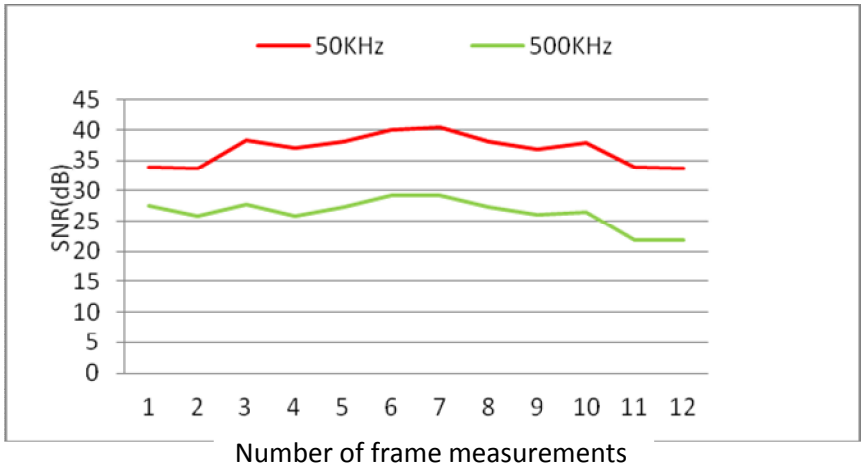

(b)

Figure 5.8 Comparison of (a) Amplitude and (b) SNR at 50 kHz and 500 kHz of single electrode combinations with no bubble

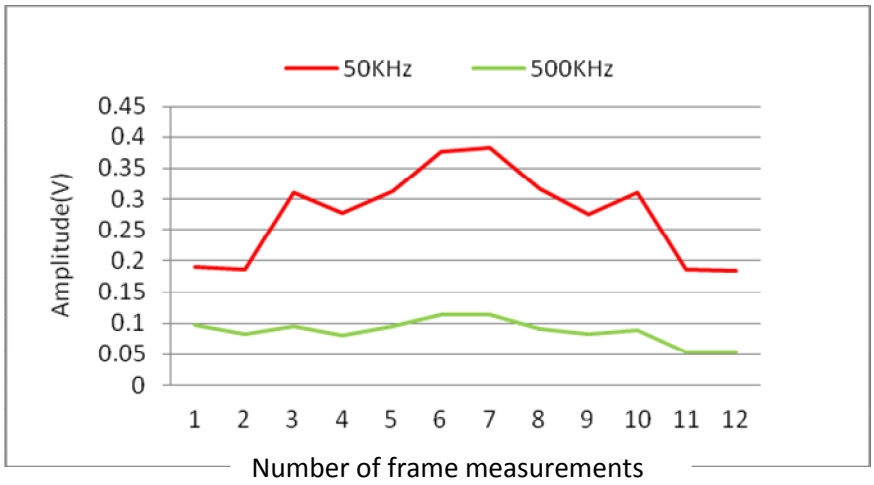

(a)

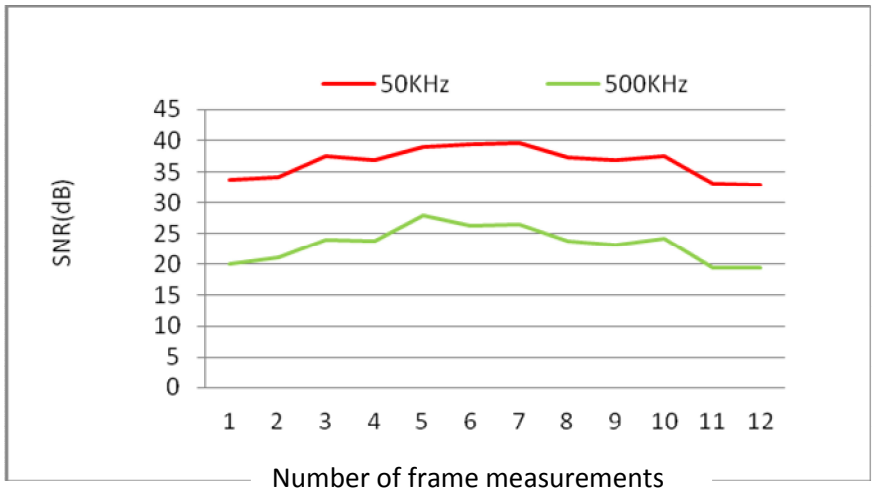

(b)

Figure 5.9 Comparison of (a) Amplitude and (b) SNR at 50 kHz and 500 kHz of single electrode combinations with 1/8 bubble

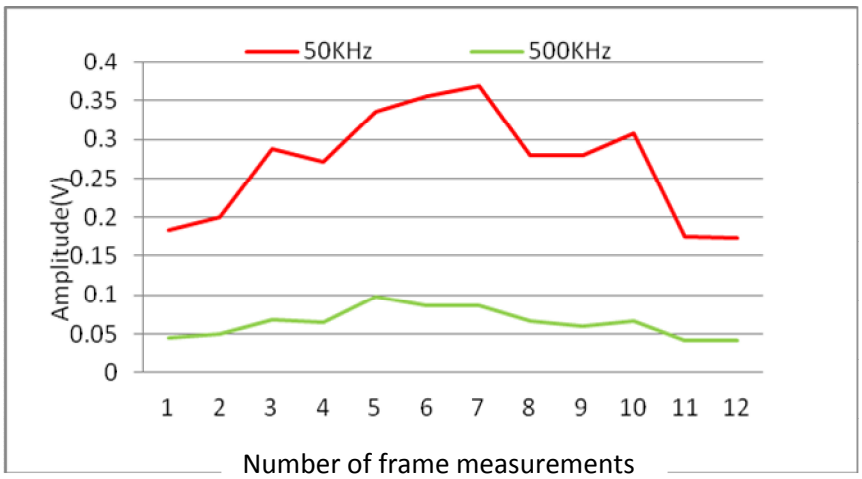

(a)

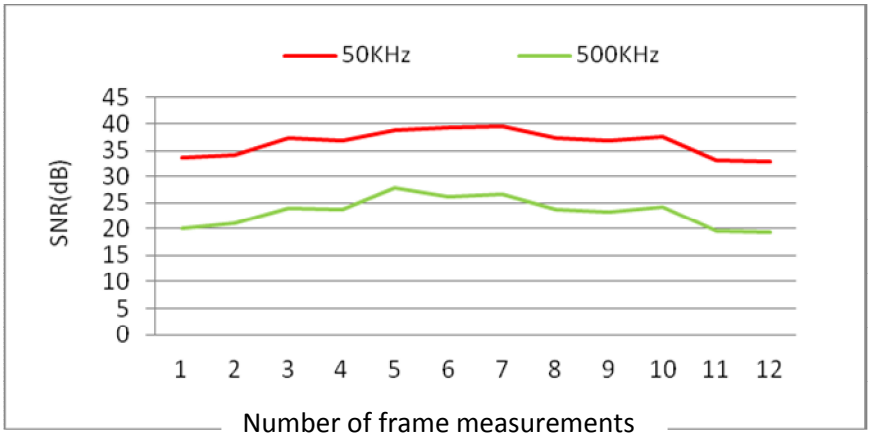

(b)

Figure 5.10 Comparison of (a) Amplitude and (b) SNR at 50 kHz and 500 kHz of single electrode combinations with 1/4th bubble

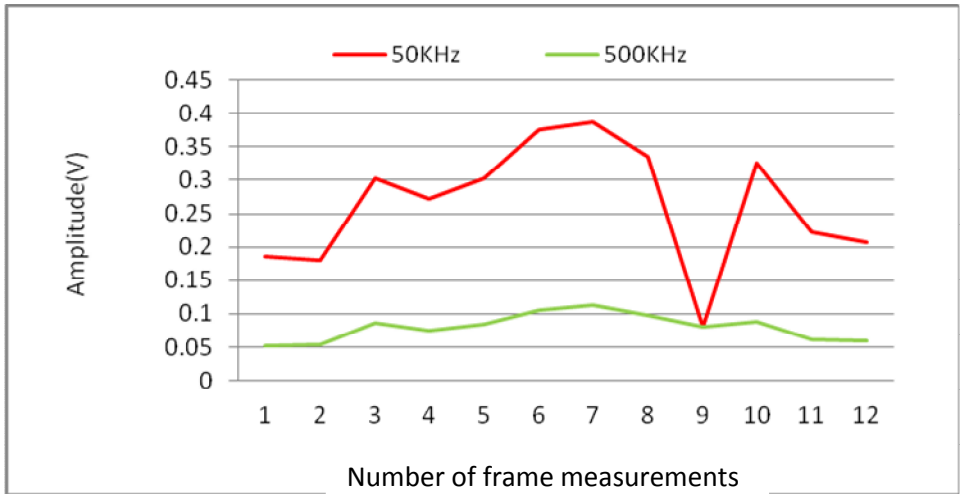

(a)

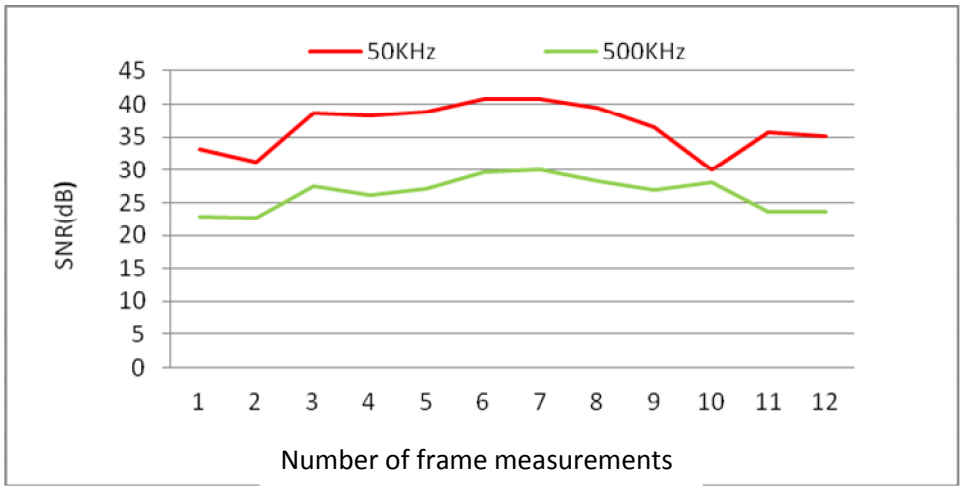

(b)

Figure 5.11 Comparison of (a) Amplitude and (b) SNR at 50 kHz and 500 kHz of single electrode combinations with 1/2 bubble

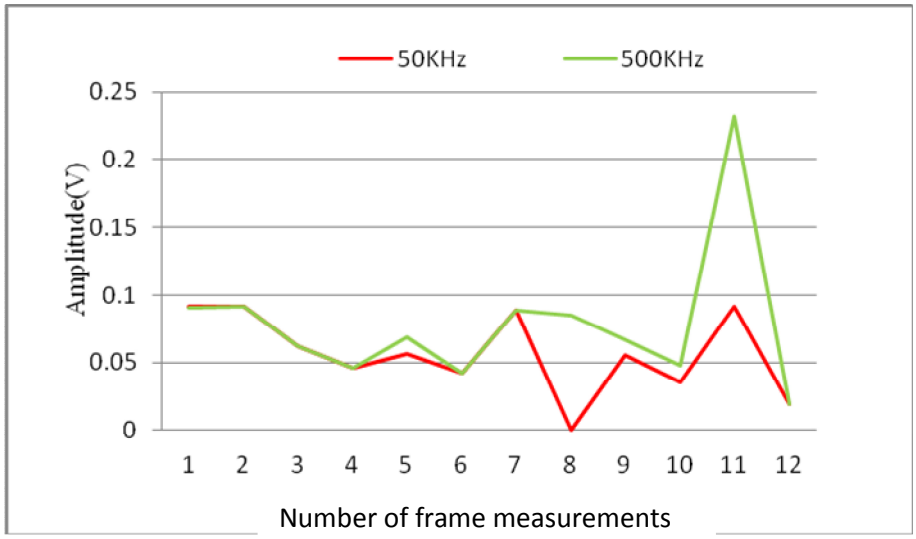

(a)

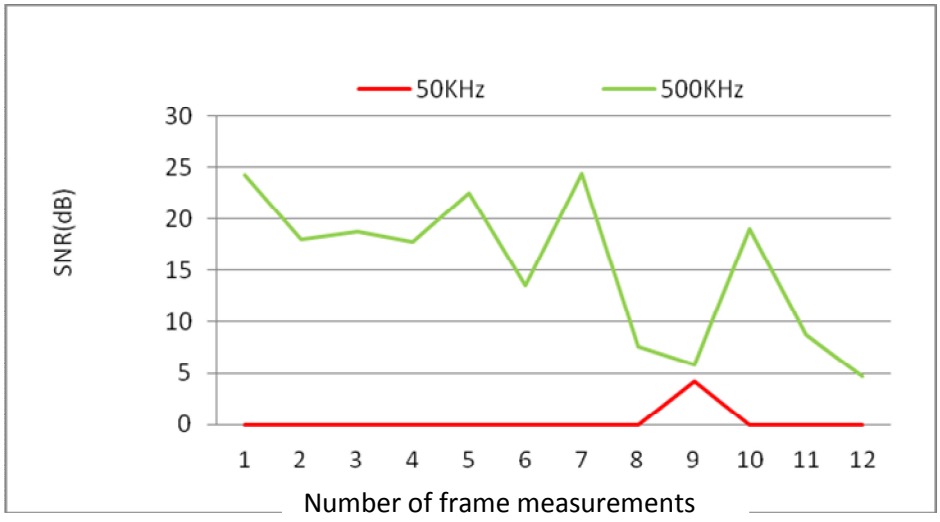

(b)

Figure 5.12 Comparison of (a) Amplitude and (b) SNR at 50 kHz and 500 kHz of single electrode combinations with full bubble

5.6.2 Symmetrical receiving electrodes

Table 5.3 Comparative analysis of SNR and voltage with different bubble sizes at 50 kHz

Bubble size	SNR_{max} (dB)	SNR_{min} (dB)	V_{max} (mV)	V_{min} (mV)
1/8th	39.49	32.98	368	174
1/4th	40.47	35.33	343	203
1/2th	40.89	31.29	387	180
Full	40.56	35.67	0.0022	179
No bubble	40.34	33.71	383	183

Table 5.4 Comparative analysis of SNR and voltage with different bubble sizes at 500kHz

Bubble size	SNR_{max} (dB)	SNR_{min} (dB)	V_{max} (mV)	V_{min} (mV)
1/8	27.84	19.39	98	42
1/4	27.84	19.38	99	42
1/2	30.12	22.74	112	51
Full	30.23	4.67	2.2	4
No bubble	29.27	21.82	115	53

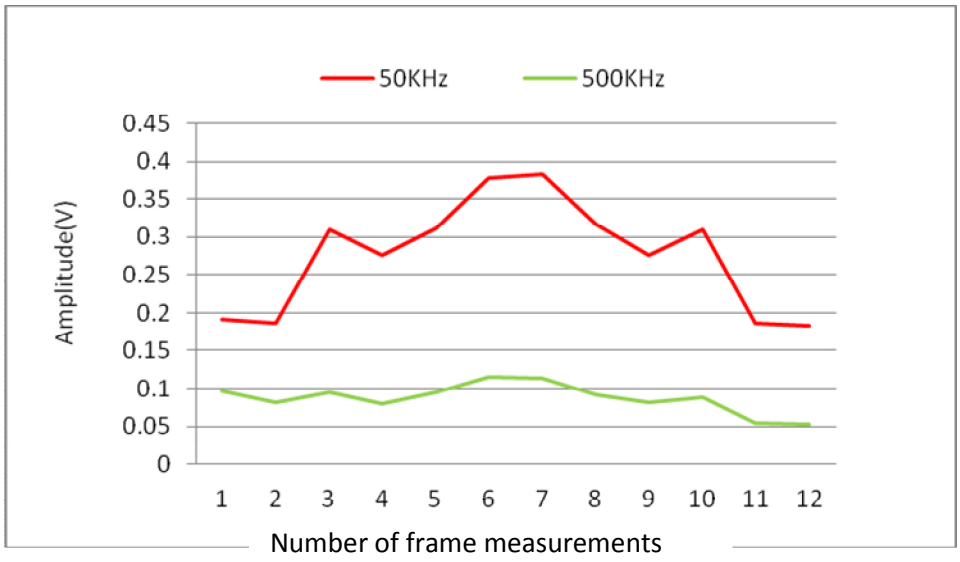

(a)

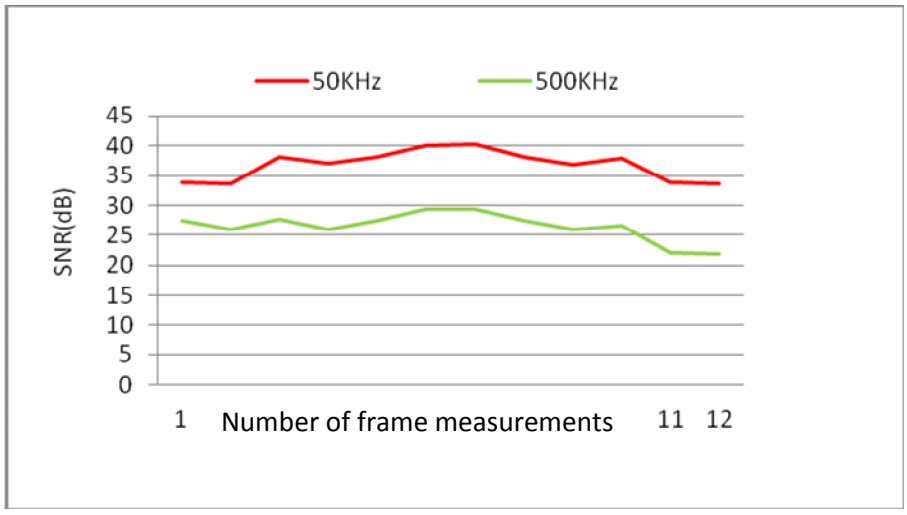

(b)

Figure 5.13 Comparison of (a) Amplitude and (b) SNR at 50 kHz and 500 kHz of single electrode combinations with no bubble

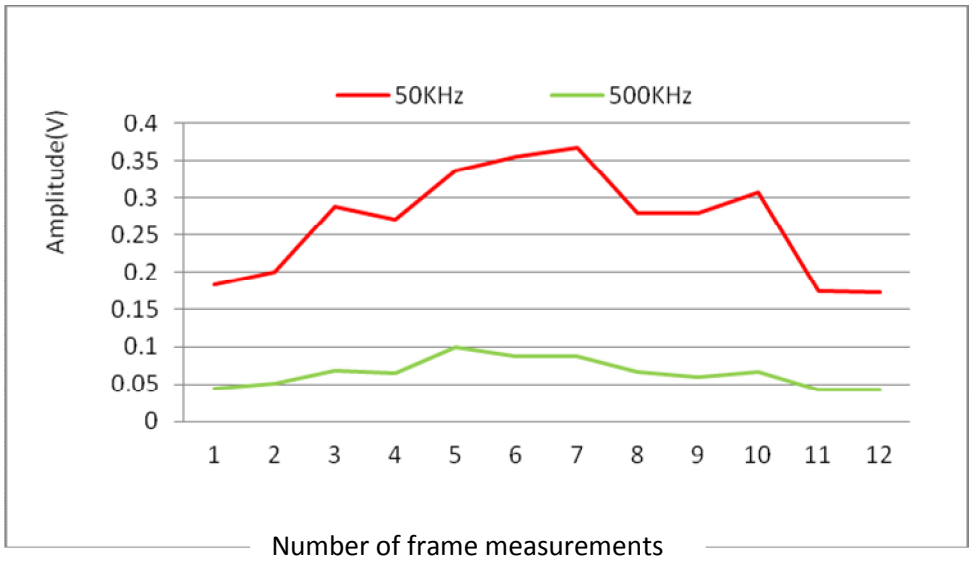

(a)

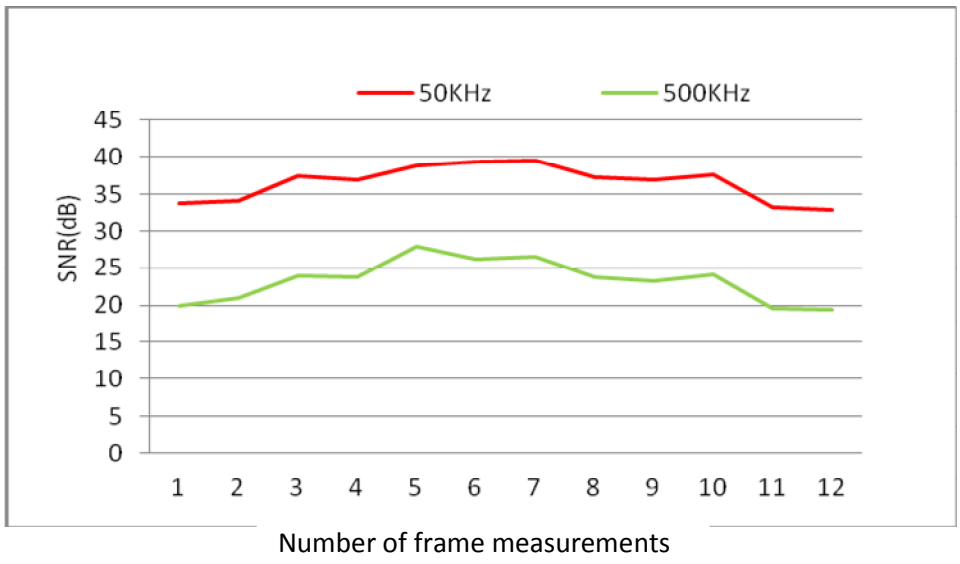

(b)

Figure 5.14.Comparison of (a) Amplitude and (b) SNR at 50 kHz and 500 kHz of single electrode combinations with 1/8 bubble

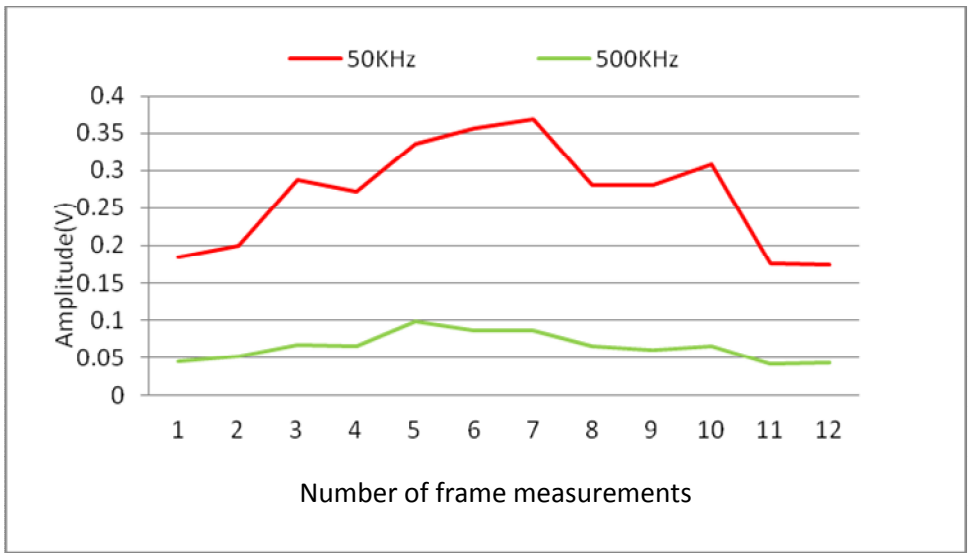

(a)

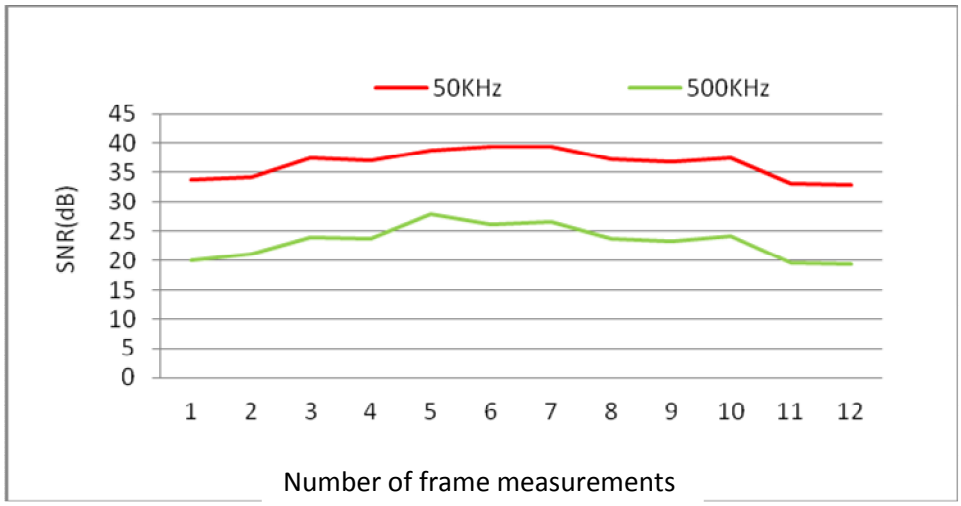

(b)

Figure 5.15 Comparison of (a) Amplitude and (b) SNR at 50 kHz and 500 kHz of single electrode combinations with 1/4 bubble

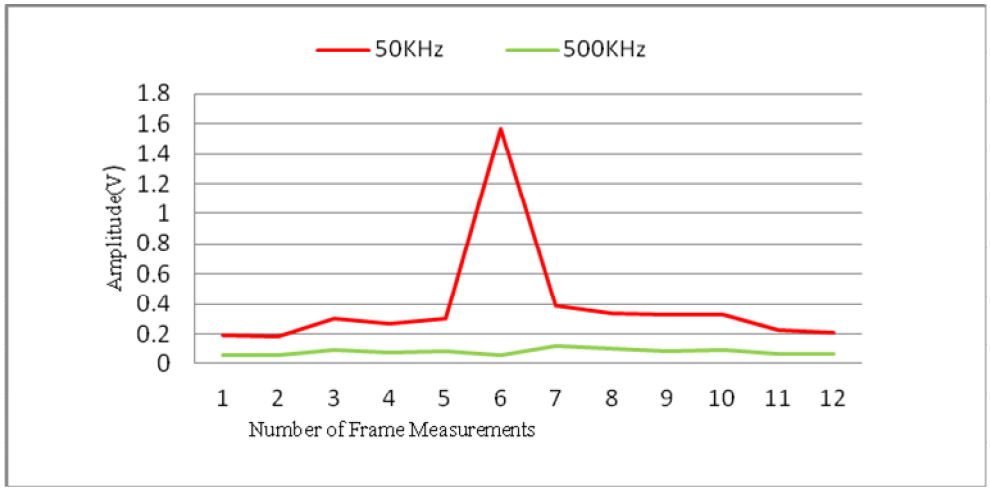

(a)

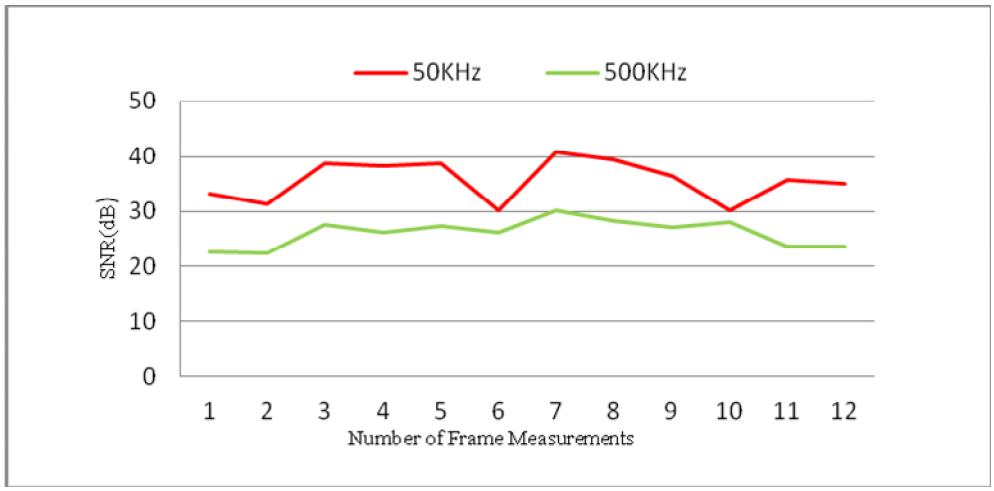

(b)

Figure 5.16 Comparison of (a) Amplitude and (b) SNR at 50 kHz and 500 kHz of single electrode combinations with 1/2 bubble

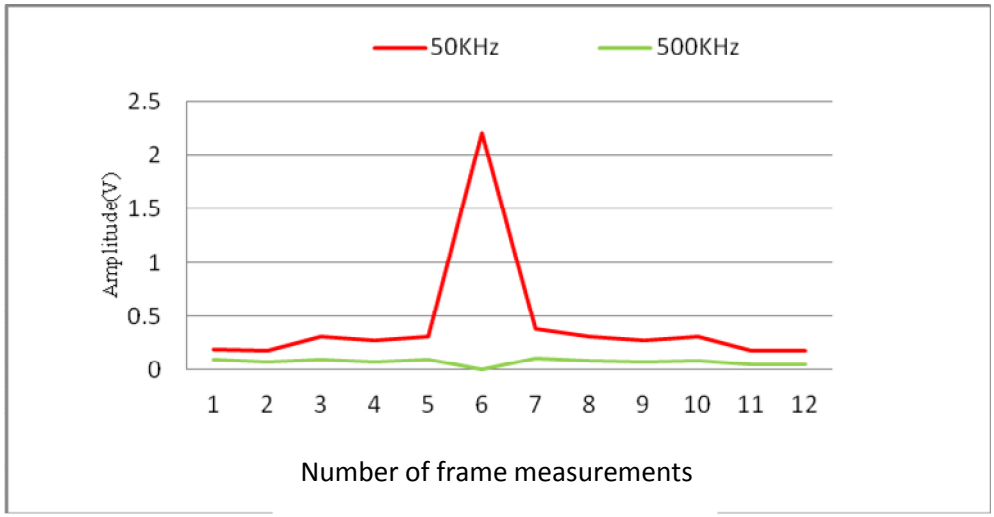

(a)

(b)

Figure 5.17 Comparison of (a) Amplitude and (b) SNR at 50 kHz and 500 kHz of single electrode combinations with full bubble

Undesired threshold voltage levels between the acquired symmetrical and non-symmetrical measurement frames introduce artefacts in the reconstructed conductivity images.

From the results shown in Figures 5.12 a) and b), 5.16 a) and b) and 5.17 a) and b), it is clear that the maximum impedance, causing the voltage threshold levels to drift to abnormality, is generated by the fully and half blocked electrodes of 2mm diameter.

Results of Figure 5.12 a) and b) show that infinite impedance has been introduced due to the fully blocked driving electrode. A bubble completely blocking a drive electrode will affect current production (since air is an insulator) thus resulting in negligible or zero signal being applied responsible for the receiving frame only recording noise or a minimum signal (approximately 0V).

Responses studied at 50 kHz and 500 kHz indicate the same characteristics of undesired threshold levels, as indicated in Table 5.1 and Table 5.2.

Artificially introduced driving electrode blocking does seem responsible for the abnormal measurements when the electrode is fully covered but does not indicate any undesired effects in Figures 5.9 a) and b), 5.10 a) and b) and 5.11 a) and b) corresponding to 1/8, 1/4 and 1/2 of the electrode diameter covered, respectively. The acquired voltage levels with these ratios of electrode covering are more or less similar to those with no bubble, with results in Figure 5.8 a) and b). This indicates that infinite impedance is only introduced when the driving electrode is fully blocked.

Results shown in Figures 5.16 a) and b) and 5.17 a) and b) show the acquired threshold levels with the half and fully blocked receiving electrodes, respectively. Saturated response can be observed on position 6 in the measurement frame shown in Figure 5.17 a) and b). This saturated response on position 6 is due to the high impedance introduced in the form of a bubble blocking completely the 2 mm acquiring surface. The high impedance point will take an abnormally high voltage drop, referred to as a saturated response in our system. The same position 6 in the frame of Figure 5.16 a) and b) also indicates the saturated response but with the threshold level half of that of position 6 of Figure 5.17 a) and b). As in the case of Figure 5.16 a) and b), the receiving electrode blockage shows that the high impedance resulting from it being covered by half a

diameter seems to have a more definite effect as compared to a half blocked driving electrode, shown in Figure 5.11 a) and b).

Figures 5.14 a) and b) and 5.15 a) and b), correspond to 1/8 and 1/4 of the electrode diameter covered, respectively. The acquired voltage levels with these ratios of electrode blockage are more or less similar to that with no bubble as shown in Figure 5.13 a) and b). Summarised results can be observed in Table 5.3 and Table 5.4.

5.6.3 Comparative analysis-symmetrical and non-symmetrical driving frame

Table 5.5 shows the voltage level values of a symmetrical frame for the driving electrode due to the injection of different bubble sizes and Figure 5.18 gives the comparison of the acquired voltages with respect to the different bubble sizes.

Table 5.5 The voltage level of symmetrical frame on driving electrode.

Electrode diameter blocked by bubble	Driving electrode	
	V_{max}(v)	V_{min}(v)
1/8	0.53	0.22
1/4	0.50	0.22
1/2	0.53	0.22
Full	2.2	0.04
No bubble	0.55	0.22

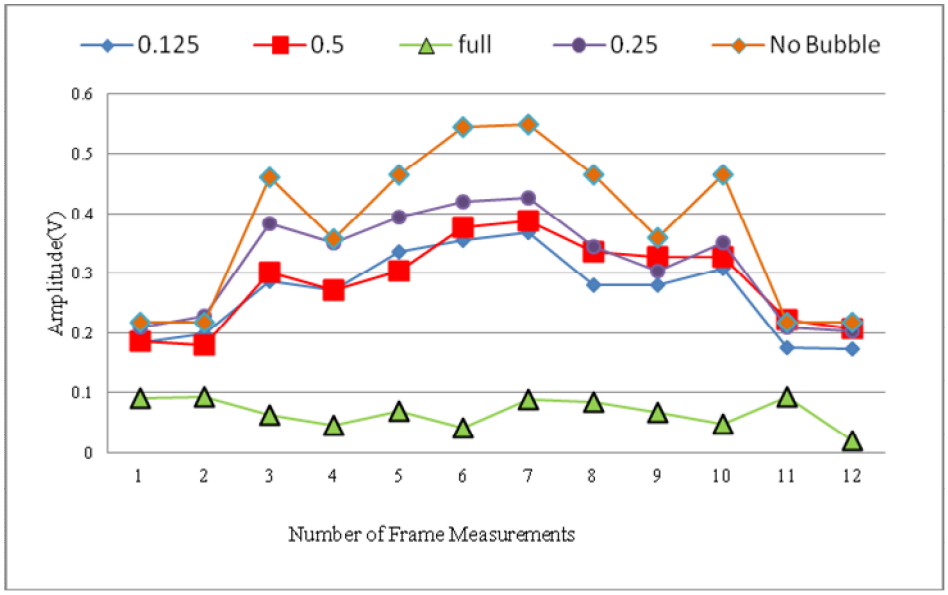

Figure 5.18 Symmetrical frame comparative analysis of raw acquired voltages with different size bubbles on driving electrodes

Table 5.6 Voltage levels of non-symmetrical frame on driving electrode

Electrode diameter blocked by bubble	Driving electrode	
	V_{max}(v)	V_{min}(v)
1/8	0.636	0.23
1/4	0.640	0.24
1/2	0.634	0.23
Full	0.636	0
No bubble	0.645	0.23

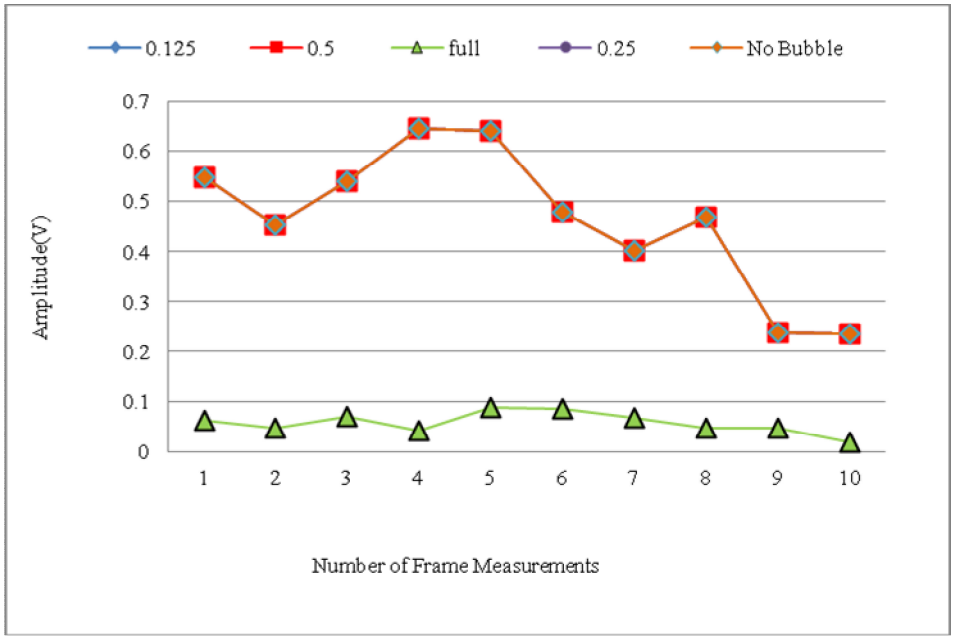

Figure 5.19 Non- symmetrical frames comparative analysis of raw acquired voltages with different size bubbles on driving electrodes.

5.6.4 Comparative analysis-symmetrical and non-symmetrical receiving frame

Table 5.7 Voltage levels of symmetrical frame on receiving electrode.

Electrode diameter blocked by bubble	Receiving electrode	
	V_{max}(v)	V_{min}(v)
1/8	0.53	0.22
1/4	0.50	0.22
1/2	1.52	0.22
Full	2.2	0.22
No bubble	0.55	0.22

Figure 5.20 shows the voltage levels at the receiving electrode with the injection of different bubble sizes.

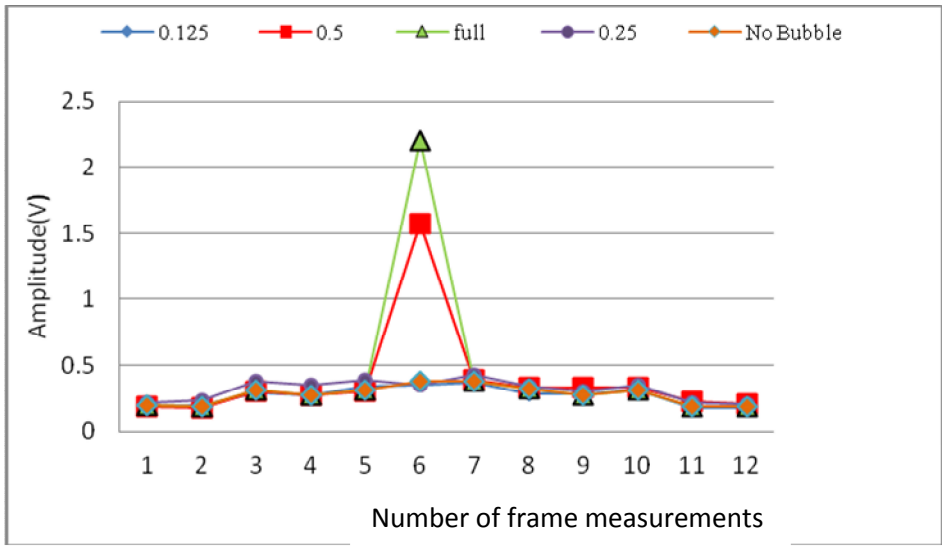

Figure 5.20 Symmetrical frame comparative analysis of raw acquired voltages with different size bubbles on receiving electrodes.

Table 5.8 Voltage levels of non- symmetrical frame on receiving electrode.

Electrode diameter blocked by bubble	Receiving electrode	
	V_{max}(v)	V_{min}(v)
1/8	0.636	0.23
1/4	0.640	0.24
1/2	0.634	0.23
Full	0.636	0
No Bubble	0.645	0.23

Figure 5.21 Non-symmetrical frame comparative analyses of raw acquired voltages with different size bubbles on receiving electrodes.

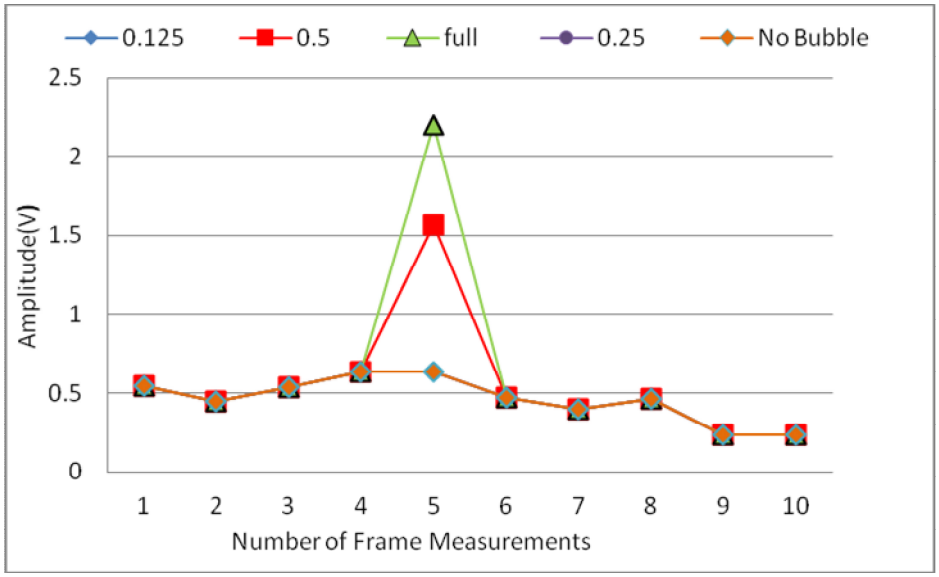

Figure 5.21 Non-symmetrical frame comparative analysis of raw acquired voltages with different size bubbles on receiving electrodes.

For both symmetrical and non-symmetrical sets of frames, the analysis of the bubbles on the receiving electrode thus shows that the bubbles covering 1/8 and 1/4 of the electrode diameter do not introduce notable impedance, in contrast to the electrodes that are half and fully blocked. A bubble covering a full receiving electrode will introduce very high impedance, resulting in a very large voltage drop (to saturation) and the voltage measured by the receiving frame will be very small, or almost zero, for the fully blocked driving electrode.

Non symmetrical frames tend to be on the corners and any abnormal affect does not appear to affect the whole measurement frame. Due to the non-symmetrical nature of the frames on the corners, breast localisation somewhere in the middle of the planar array electrode is important. Symmetrical frames have 12 measurement points and are considered to be in the central area.

5.7 Conclusion

For both symmetrical and non-symmetrical sets of frames, the analysis of the bubbles on the receiving electrode thus shows that the bubbles covering 1/8 and 1/4 of the electrode diameter do not introduce notable impedance, in contrast to the electrodes that are half and fully blocked. A bubble covering a full receiving electrode will introduce very high impedance, resulting in a very large voltage drop (to saturation) and the voltage measured by the receiving frame will be very small, or almost zero, for the fully blocked driving electrode.

Non symmetrical frames tend to be on the corners and any abnormal affect does not appear to affect the whole measurement frame. Due to the non-symmetrical nature of the frames on the corners, breast localisation somewhere in the middle of the planar array electrode is important.

5 .8 Summary

In this chapter an overview of the possible causes of undesired in-vivo threshold voltage levels is discussed in detail. This study includes a number of possible factors a comprehensive study and analysis of what ratio of electrode blockage can affect the acquired raw data compromising reconstruction that follows.

The next chapter concentrates on the methods to mitigate unwanted affects and techniques for fast detection of any such occurrences.

Chapter 6 Methods to mitigate undesired voltage threshold levels in an EIT planar array system for in-vivo breast cancer

6.1 Introduction

In the previous chapter, an outline of the types of electrode blockage together with what ratio of electrode coverage will affect the acquired voltage is given. In this section methods to mitigate these factors are discussed. Undesired threshold voltage levels between the acquired measurement frames will cause artefacts to be introduced in the reconstructed conductivity images. However, these abnormal threshold levels are not replaced by appropriate information using software calibration before reconstructing the conductivity images. Due to this fact, the occurrence of infinite impedances leading to these abnormal measurements should be mitigated.

6.2 Purpose of this study

Prior to image reconstruction for the detection of breast cancer, it is important to remove and replace very low and high potentials and improve the SNR of the acquired signal. In the Sussex Mk4 EIM System this task is achieved by using Matlab software. It can be termed as a pre-calibration procedure as explained in Figure 6.1 and Figure 6.2.

In the Sussex EIM System, minimum and maximum potentials i.e. <10mV (termed as "dead channels") and $\geq 20V$ (termed as "saturated channels") are removed before reconstruction. Using software, dead channel measurements and/or saturated channels measurements are replaced by the preceding or following channel measurements.

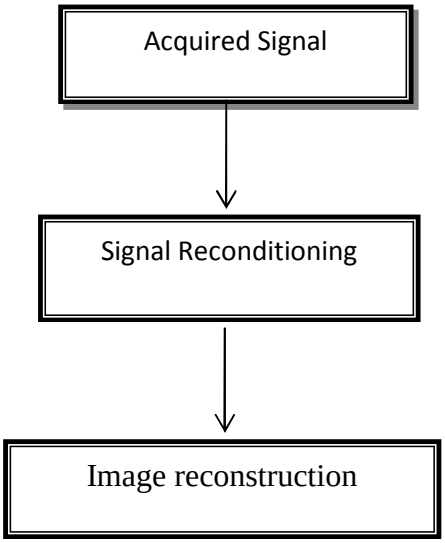

Figure 6.1 Block diagram representation of steps involved in image reconstruction

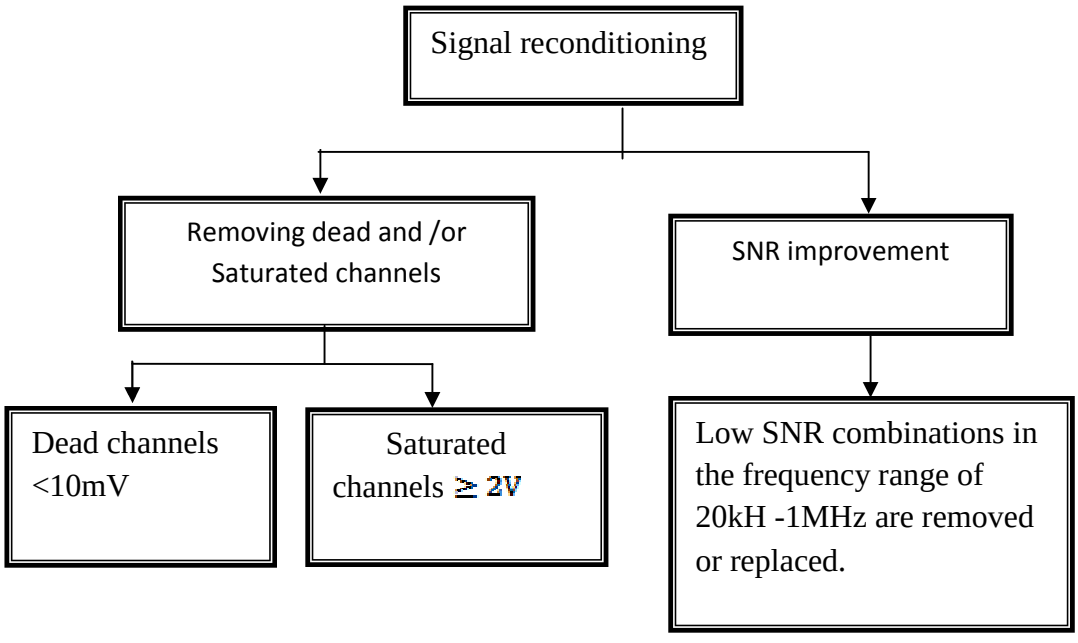

Figure 6.2 Software calibration block diagram

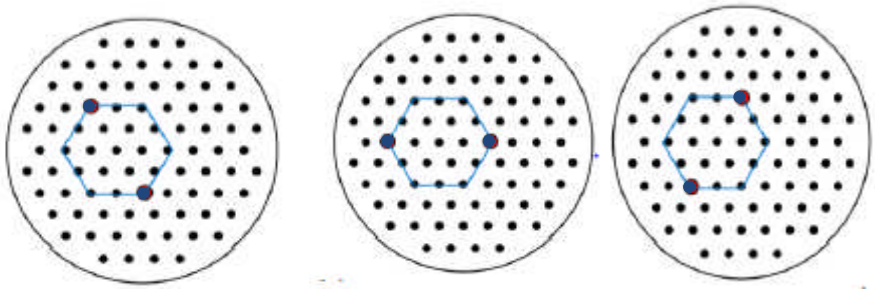

(a) (b) (c)

Figure 6.3 Sussex Mk4 planar array driving hexagon frame (in blue) with (a) driving electrode blocked (in red) (b) to be replaced by a preceding frame or (c) following frame(Sze *et al* 2011).

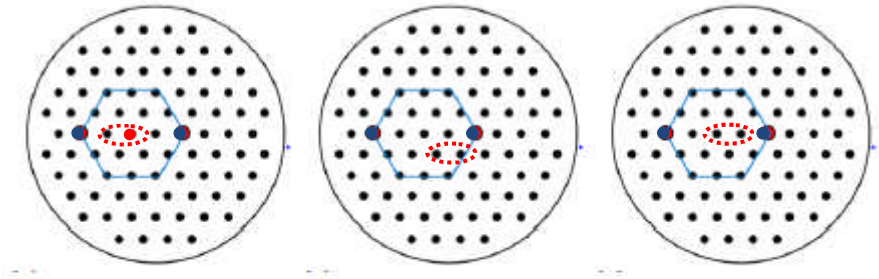

(a) (b) (c)

Figure 6.4 Sussex Mk4 planar array driving hexagon frame (in blue) with: (a) single receiving electrode blocked (in red) (b) to be replaced by a preceding single measurement (in dotted red) or (c) following single measurement (dotted red)

Having a minimum threshold voltage (<10mV) means a whole frame of 10-12 measurements loss as a result of a particular driving electrode blockage and a maximum threshold at a particular receiving combination indicates the loss of a single measurement.

Single and whole frame replacement by the latter or former channel and/or frame is not an appropriate information swap. Figure 6.3 (a), (b) and (c) show the frame replacement and Figure 6.4 (a), (b) and (c) indicate single measurement replacement.

Following are the possible methods to reduce unwanted threshold voltage levels until some appropriate solution of swapping these measurements is devised. This includes a

comprehensive investigation to reduce saline displacement. Also, possible patient introduced systematic errors are discussed.

6.3 Fast sweep method for the electrode blockage detection

The combination pattern shown in Figure 6.5 is used to scan the plate and indicate the affected blocked pin due bubbles, debris or skin.

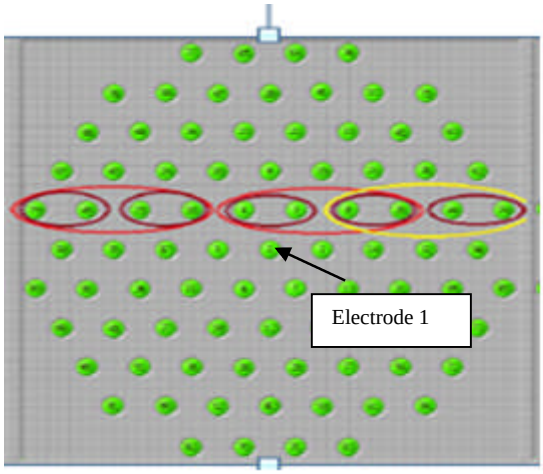

Figure 6.5 Electrode plate and combination pattern (Beqo *et al* 2011)

A flat response is expected if only saline is present in the system as shown in Figure 6.7. To test this supposition, an air bubble was artificially introduced on top of electrode 1 shown in Figure 6.5 and Figure 6.6. The acquisition was done at low frequencies. Distortion can be seen on combination 25 (positive) and 26 (negative) in Figure 6.8.

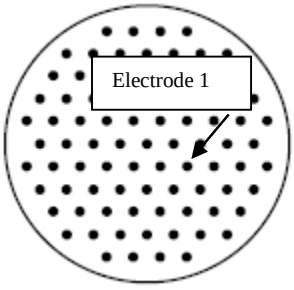

Figure 6.6 Electrode 1 indicated

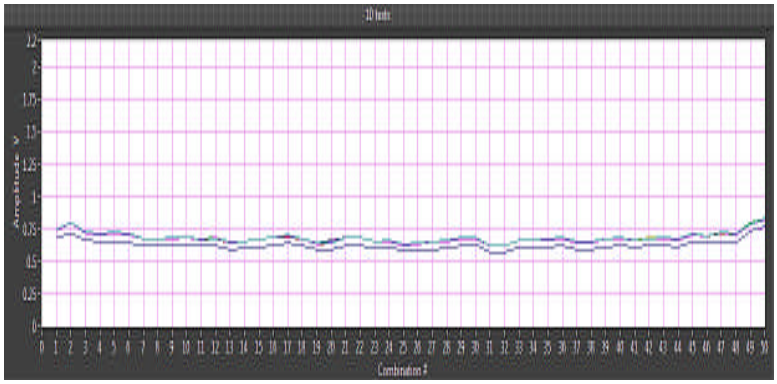

Figure 6.7 Flat responses in saline with no electrode blocked (Beqo *et al* 2011).

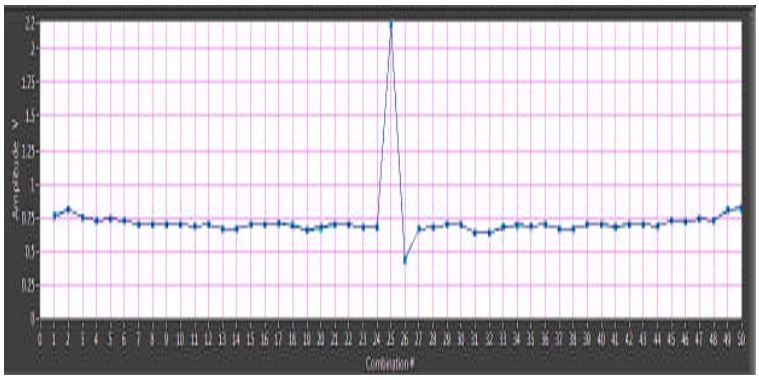

Figure 6.8 High impedance detected on electrode 1 from same condition in Figure 6.7(Beqo *et al* 2011).

The magnitude of the signal can be used to identify how covered the electrode is (i.e. how big the bubble is) and map where the breast is touching. The 1416 combinations have been reduced to 50, where all the pins alternate into drive and receive using the same distance in every combination. The scan is done at low frequencies as the Mk4 response is best at 50 kHz and 100 kHz.

Figure 6.9 Water filled balloon in the scanner head for scanning (Beqo *et al* 2011).

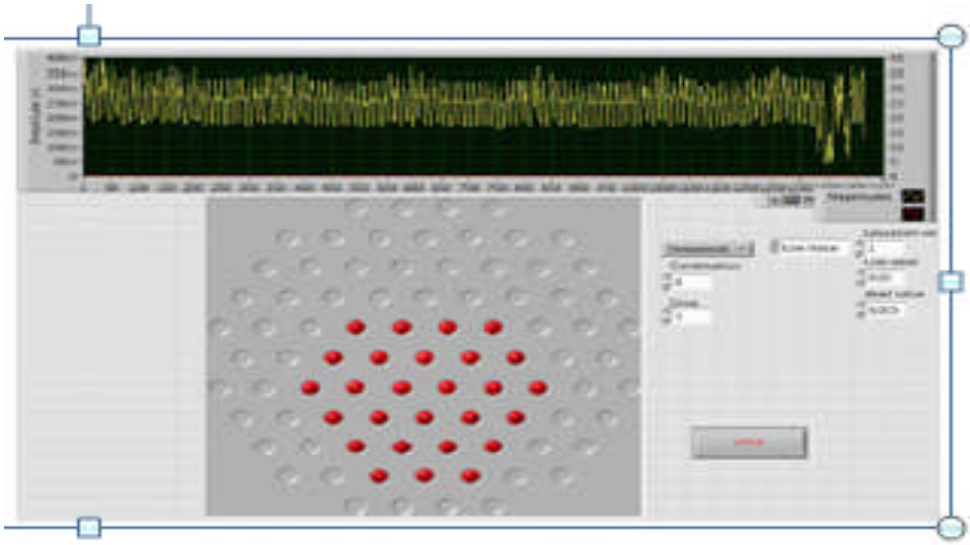

Figure 6.10 Balloon map with fast acquisition (Beqo *et al* 2011).

6.4 Mitigating possible electrode blockage due to patient introduced errors

While analysing the acquired data it is noticed that at certain electrode combinations the acquired signal response is saturated and/or very low amplitude. This response changes with the volunteers indicating that patient introduced factors are also playing part in these abnormal measurements. Possible factors discussed earlier can be reduced by using the following methodologies.

6.4 1 Dry skin

The skin is properly moistened before scanning in order to avoid bubbles being generated through dry skin at the saline interface. Baby wipes have been used to moisten as a standard "skin conditioning procedure" before scanning, avoiding bubble formation. The non-conductive and non-adhesive nature of the wipes will not contribute any adverse effect to the acquired signal.

6.4.2 Saline displacement due to skin and weight

It is also observed that the subject's skin and weight removes the contact medium by displacing the saline from the electrodes. Saline displacement will cause the electrode to block and is responsible for the low density current due to infinite impedance at that point. Different experiments are carried out to reduce the saline displacement which is discussed in detail later in the chapter.

6.5 Reducing saline displacement due to skin and weight

The problem of saline displacement is verified by an experiment done with a transparent water filled balloon as shown in Figure 6.5. A filled balloon was used to study the effect of displacement caused by the breast skin and weight. It was observed that the skin and weight of the balloon removes the contact medium by displacing the saline from the electrodes. Also electrode blocking by simply using one’s fingers produced the same results of creating a saturated and dead channel.

6.5.1 Different protocol analysis for avoiding saline displacement due to skin and weight

Several experiments are carried out using different protocols to minimise saline displacement from the electrodes. The aim is to use a method that will form a constant saline layer between the subject and the electrode but at the same time produce a response closer to that of the original electrode plate. Protocols used for the experiments include medical ring gauze and ridges. In-vitro tests of the gauze on the patient showed that if

not placed correctly the gauze would move, causing a fold to disrupt the attempt to produce a uniform layer. Improvements to the gauze positioning are introduced by means of an acrylic ring that keeps the gauze constantly tight and in a perfect un-foldable layer. Also, a ridged plate was tested for this purpose. From a calibration point of view, the SNR, dynamic range and impedance introduced by a suitable protocol should be identical or close to that of the original plate.

Impedance introduction is one of the most important factors studied for the protocols used to eliminate or minimise saline displacement. The concept is to avoid introducing noticeable impedance within the scanner head that could shunt the subject being scanned. By shunting is meant directing current to flow from the lower resistive path, i.e. the protocol introduced to avoid displacement, rather than going through the patient's skin, which is clearly not desired.

The SNR of the acquired signal with the protocols should be sufficient and not lower than the original plate for image reconstruction. The SNR of the system is around 40-45dB between 50-100 kHz which is acceptable, though this depreciates at higher frequencies (which are not considered for the image reconstruction).

The dynamic range should be minimal with electrodes having a large to maximum potential. The dynamic range for the Sussex Mk4 EIM system is in the range of 2.10 - 2.33.

6.5.2 Plain plate

Acquisition using back projection and 2D Impedance mapping is shown in Figure 6.11 (c) and Figure 6.11 (b) respectively using the plain plate shown in Figure 6.11 (a).Parameters to be analysed are summarised in Table 6.1.

Table 6.1 Plain plate parameters

Z_{max} (Ω)	V_{max} (mV)	V_{min} (mV)	SNR_{max} (dB)	Dynamic Range
0.3616	490	190	43	2.32

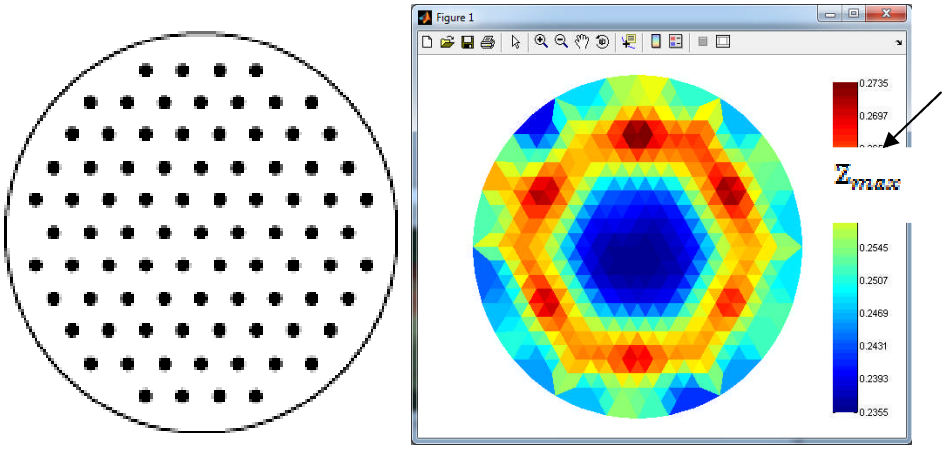

(a) (b)

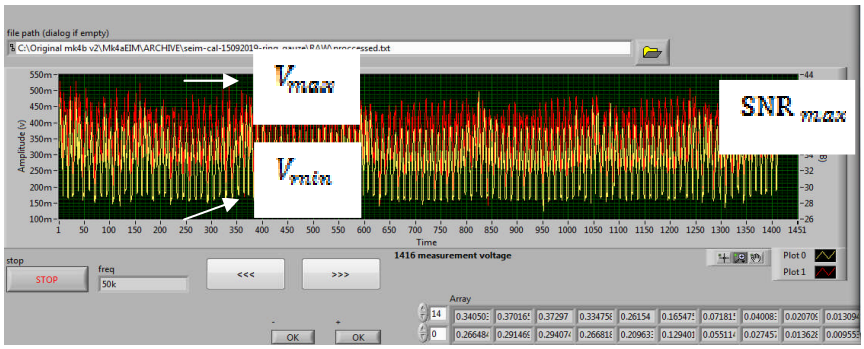

(c)

Figure 6.11 (a) Picture of plain plate (b) 2D Impedance map indicating Z_{max} (c) Acquired signal with plain plate showing V_{max} and V_{min}(yellow waveform) and SNR_{max}(red waveform).

6.5.3 Gauze

Acquisition using back projection and 2D Impedance mapping is shown in Figure 6.12 (c) and Figure 6.12 (b), respectively, using the saturated medical gauze shown in Figure 6.12 (a).Parameters to be analysed are summarised in Table 6.2.

Table 6.2 Gauze parameters

Z_{max}	V_{max}	V_{min}	SNR_{max}	Dynamic Range
(Ω)	(mV)	(mV)	(dB)	
0.2785	400	150	41	2.17

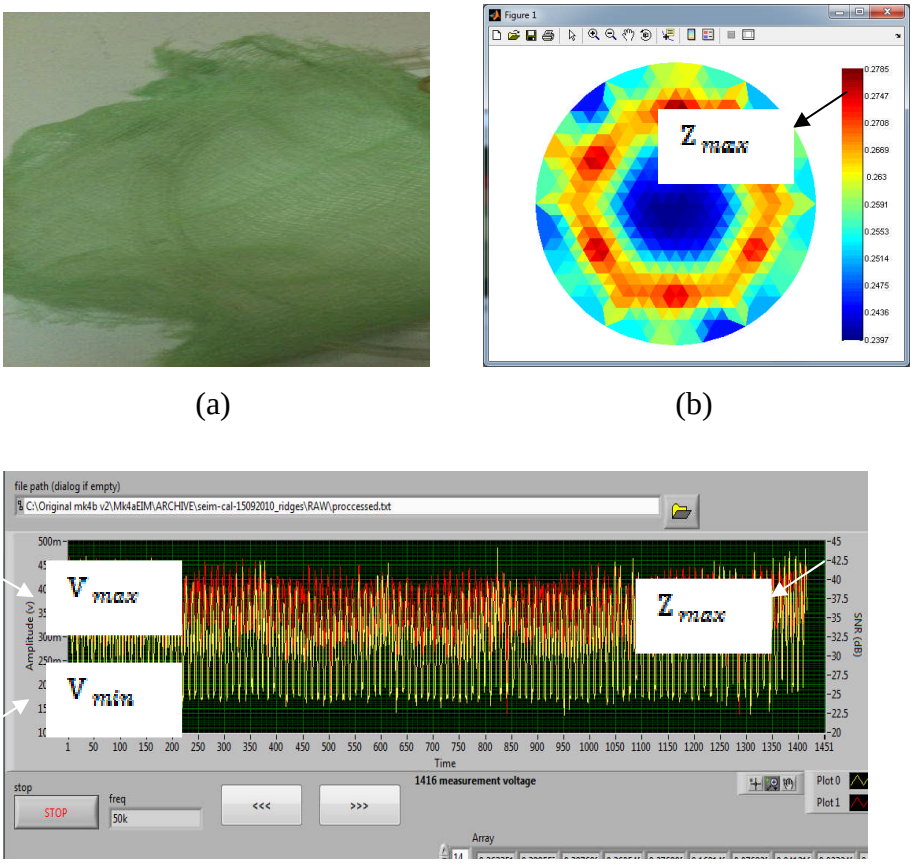

(a) (b)

(c)

Figure 6.12 (a) Picture of saline saturated medical gauze (b) 2D Impedance map indicating Z_{max} (c) Acquired signal with gauze showing V_{max} and V_{min} (yellow waveform) and SNR_{max}(red waveform)

6.5.4 Ring gauze

Acquisition using back projection and 2D Impedance mapping shown in Figure 6.13(c) and Figure 6.13 (b), respectively, using ring gauze shown in Figure 6.13 (a). Parameters to be analysed are summarised in Table 6.3.

Table 6.3 Ring gauze parameters

Z_{max}	V_{max}	V_{min}	SNR_{max}	Dynamic Range
(Ω)	(mV)	(mV)	(dB)	
0.3616	490	190	43	2.32

(a)

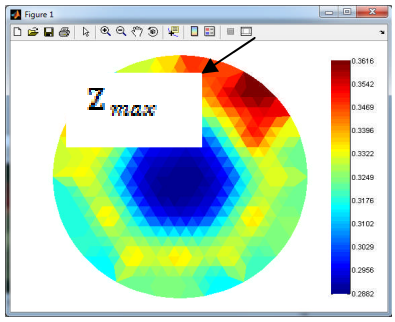

(b)

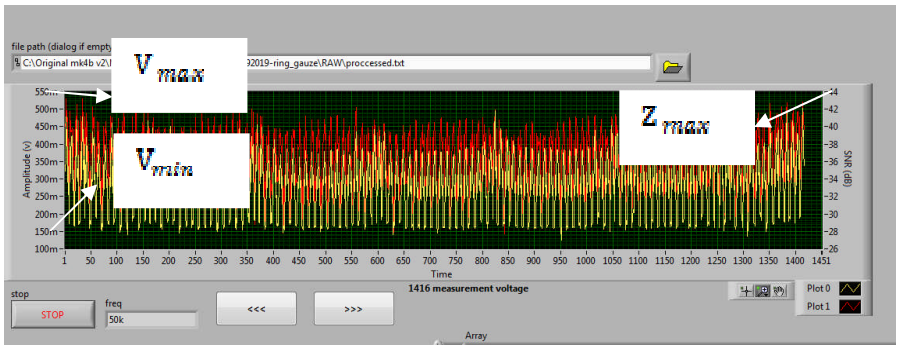

(c)

Figure 6.13 (a) Picture of ring gauze (b) 2D Impedance map indicating Z_{max} (c) Acquired signal with ring gauze showing V_{max} and V_{min}(yellow waveform) and SNR_{max}(red waveform)

6.5.5 Ridges

Acquisition using back projection and 2D Impedance mapping is shown in Figure 6.14(c) and Figure 6.14 (b), respectively, using ridges as shown in Figure 6.14 (a). Parameters to be analysed are summarised in Table 6.4.

Table 6.4 Ridges parameters

Z_{max}	V_{max}	V_{min}	SNR_{max}	Dynamic Range
(Ω)	(mV)	(mV)	(dB)	
0.3652	500	170	44	2.12

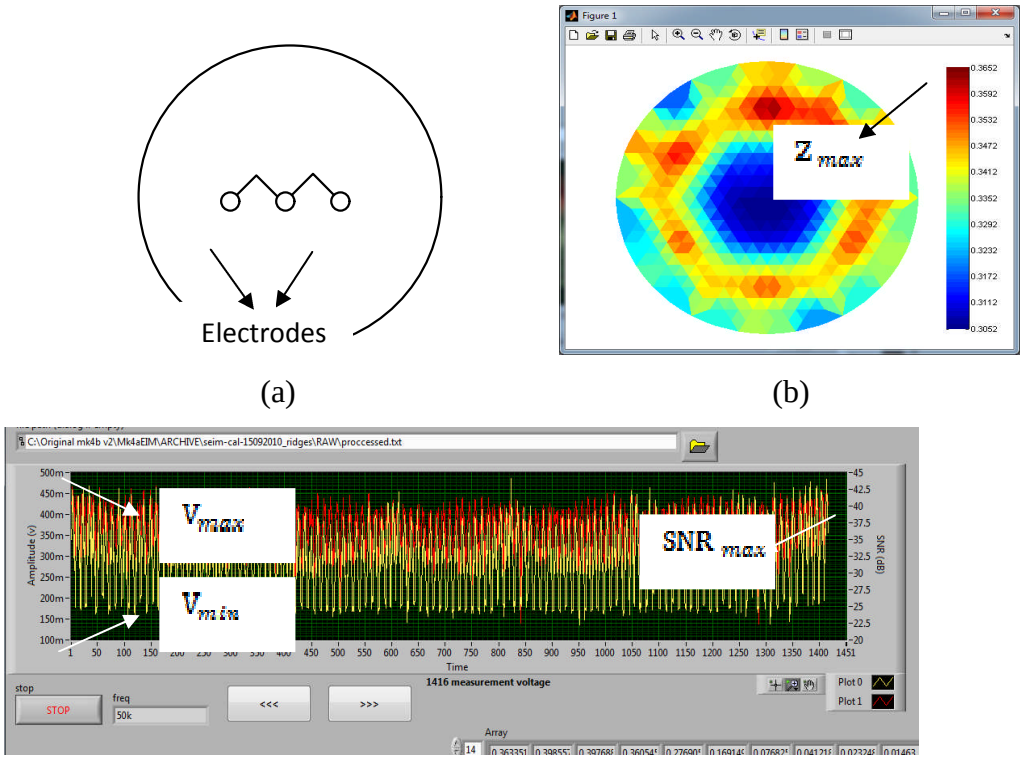

Figure 6.14 (a) Picture of ridges (b) 2D Impedance map indicating Z_{max} (c) Acquired signal with ridges showing V_{max} and V_{min}(yellow waveform) and SNR_{max}(red waveform).

6.6 Mitigating systematic errors

Bubble formation due to systematic errors including DC offset levels can be minimised so as to mitigate the artefacts appearing in the conductivity images reconstructed. The following options are worth considering for this purpose

6.6.1 Rinsing electrodes with higher surface tension liquid

Rinsing electrodes with non-conductive, high surface tension liquid does not let bubbles initially form or stay on the electrodes once formed due to micro gaps between the plate and the electrodes. For the Sussex Mk4 EIM System, cholorohexidine with 155µS of conductivity is used to avoid bubble formation and growth. The non-conductive characteristic means the scan is not affected.

6.6.2 By reducing acquisition scan time

In order to avoid bubble formation due to DC offset, the scanning time per breast should be reduced to deal with the bubble generation problem, in return improving overall system performance.

The scanning time depends on several factors including:

i. The acquisition format used by the controlling (or acquiring) software should be the same as that of the analogue-to-digital converter (digitizer).

ii. The analogue multiplexer should have minimum ON and OFF switching times.

6.7 Mitigating EIM sensor errors

The best possible way of avoiding the artefact caused by the gaps is to fill the dry scanner head with saline solution before starting to scan a volunteer in-vivo. Bubbles due to the air pockets between the electrodes and the acrylic plate will keep on growing

until all of the air pockets are filled. This will minimise the bubble growth and generation due to electrode and electrode plate spacing.

6.8 Mitigating skin plate contact

In the Sussex Mk4, the scanner head plate moves up-down to accommodate different volume sizes by slightly compressing the breast and holding it steady while the patient lies on her front. The possibility of saline displacement and electrode blockage due to the patient's skin is more when the breast is pressed against the electrode plate while scanning the volunteer lying on her front, as shown in Figure 6.16.

6.8.1 Lateral scanning position

Thus a proposed change of the scanning position is to have the volunteer lie sideways in order to minimize the subject and electrode plate contact. However, lateral scanning requires further investigation.

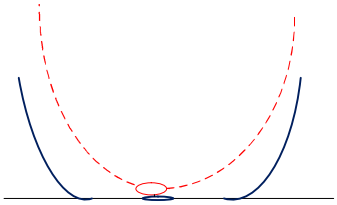

Figure 6.15 Comparison of subject model - patient lying on front (blue) and lateral (red)

6.8.2 Redefining depths

Hence by adjusting the scanner head depth 1 or 2 mm more than that of the subject's volume can reduce skin and electrode plate contact as shown in Figure 6.17. Table 6.6 shows different volumes corresponding to existing and suggested depths.

Table 6.6 Different volumes corresponding to existing and suggested depths

Different volumes	Existing Mk4 depth (mm)	Suggested depth (mm)
AA	5	6

A	10	11
B	16	17
C	18	19
D	26	27
E	32	31
F	40	39
G	45	44

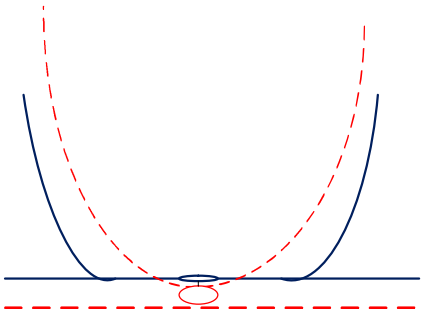

Figure 6.16 Dotted red lines show redefined breast volume depths whereas blue indicates current scanning depths.

6.9 Discussion

6.9.1 Fast sweep method

By using the fast electrode combination, the operator can be notified that the breast needs to be repositioned before the scan, in contrast to a standard acquisition followed by image reconstruction which can take a couple of minutes in which there is no fast indicative method to notify the operator.

Because there is no reconstruction involved, the mapping is instant as shown below in Figure 6.9 and Figure 6.10. A transparent party balloon filled with water is placed inside the scanner which is full of saline. Transparent balloon only used to visualise the subject in the scanner condition to see through confirming the displaced saline from the electrodes. Balloon material is not at all conductive and cannot mimic breast skin and fat.

The software Acquire-Map acquisition time is 4 seconds. The balloon is moved around the scanner to see that the identical response corresponding to the new position is displayed as shown in Figure 6.10.

The scan takes a couple of seconds and provides live feedback from on the electrode map. Taking into consideration the amount of minutes it takes for a full acquisition and reconstruction, this dynamic scan method can help in patient positioning, as shown in Figure 6.10.

6.9.2 Mitigating patient introduced errors

Dry skin can cause bubbles to be generated due to the dry skin and the saline interface. Skin conditioning procedure will not contribute any adverse effect to the acquired signal.

6.9.3 Saline displacement due to skin and weight-different protocol analysis

Keeping the key points discussed in section 6.5.1 in mind and the results shown in the comparative Table 6.5, it can be seen that gauze is the most suitable medium that can be employed to avoid saline displacement. Medical cotton gauze fully immersed in a dielectric medium creates a constant layer of saline medium. Because the gauze fully saturates with saline, its response is almost transparent to an electrical field, thus not introducing impedance. The response of the ring gauze and ridges are very similar in terms of the acquired voltage levels, SNR and impedance introduced. It has been shown that the ring gauze introduces high impedance when scanned without gauze.

As far as the response of the ridges is concerned, high impedance might be due to the fact that the grooved plate was kept on top of the original electrode plate, the embedding allowing the saline medium to be in between the original plate and the ridges. The saline medium underneath the ridges has possibly introduced a shunt, appearing as a parallel load. It has yet to be tested whether the grooved plate fixed within the scanner head returns a similar response as far as introduced impedance is concerned, or some other effect.

Table 6.5 Comparison of different protocols for saline displacement

	Z_{max} (Ω)	V_{max} (mV)	V_{min} (mV)	SNR_{max} (dB)	Dynamic range
plain plate	0.3616	490	190	43	2.32
with gauze	0.2785	400	150	41	2.17
with ring gauze	0.3616	490	190	43	2.32
with ridges	0.3652	500	170	44	2.12

6.9.4 Mitigating systematic errors

Bubble formation due to systematic errors including DC offset levels can be minimised by rinsing the electrodes with non-conductive, high surface tension liquid. For the Sussex Mk4 EIM System, cholorohexidine with 155µS of conductivity is used to avoid bubble formation and growth. The non-conductive characteristic does not affect the scan.

Another solution to avoid bubble formation due to DC offset is to reduce the scanning time and by using minimum ON and OFF switching time analogue multiplexer. The scanning time depends on several factors including the acquisition format used by the controlling (or acquiring) software and the digitizer.

6.9.5 Mitigating EIM sensor errors

Bubbles due to the air pockets between the electrodes and the acrylic plate can be avoided by filling in the dry scanner head with saline before scanning a volunteer.

6.9.6 Mitigating subject plate contact

Thus a proposed change of the scanning position discussed earlier in the chapter is to have the volunteer lie sideways in order to minimize the subject and electrode plate contact. However, lateral scanning requires further investigation.

Moreover, subject plate contact can be reduced by scanning the 1 or 2 mm greater than the current settings. For example, volume currently scanned with 18mm depth should be

scanned at 19 or 20 mm depth. Further investigation is needed as to how the existing specific depths are calculated and chosen.

6.10 Conclusion

Unwanted voltage levels can be identified by using the electrode combination patterns and the sweep method of acquisition. The sweep method can be a fast solution to identify any artefact or foreign objects on the pins. The proposed methodologies presented in this chapter will not only prevent the possibility of bubble generation but also electrode blockage due to the patient's skin and so provide a large step forward in allowing significant improvement of EIM imaging for possible cancer detection. The future work will optimise the above methodologies for a wider range of female populations under different conditions for incorporation into the EIM data quality control software routines.

6.11 Summary

In this chapter possible methods to reduce unwanted threshold voltage levels are proposed. This undesired threshold levels are responsible for introducing artefacts in the reconstructed conductivity images. This research also includes a comprehensive investigation to reduce saline displacement along with the patient introduced errors.

Chapter 7 Conclusions and suggestions for future work

7.1 Introduction

In this final chapter the conclusions from this breast cancer diagnosis system are presented together with suggestions for further research work.

7.2 Summary of analysis, methodologies and results

There are several sources of errors affecting system performance and image quality and these are categorized and discussed in detail in this research. The categorization of artefacts is done on the basis of systematic factors degrading the acquired response, externally introduced sources of errors responsible for affecting image quality, and predictable and unpredictable noise responsible for limiting system performance over a wide range of bandwidth and so degrading image quality.

Systematic sources of errors may include the hardware circuit layout i.e. current source and multiplexer configuration, analogue multiplexer switch ON and OFF capacitances and resistances, high output impedance current sources over a wide range of frequencies and stray capacitance due to PCB tracks.

Other artefacts considered that degrade image quality are treated separately as patient introduced and due to hardware configuration errors.

Predictable and unpredictable noises introduce frequency dependent noise levels degrading the detected voltage levels.

Predictable noise due to internal electronic circuitry is repeatable and remains at the same level irrespective of the input. This could cause frequency dependent DC offset and phase shifts within the measured signal and act as a low pass filter. This low pass effect will change the magnitude of the received signal at different frequencies. As image reconstruction is based on the voltages measured from the electrodes, the smaller the voltages are, the more influence small amounts of noise will have. Noise in the present Sussex EIM acquisition system is between 20 and 30 dB.

Unpredictable noise sources are random in nature. They cannot be predicted or repeated. External noise in the MK4 EIM System used for the clinical environment in any hospital, includes artefacts caused by patient movement and room wall banging due to close proximity of X-Ray CT scanning. This results in a sudden change to the detected measurement. Most of the external sources are random and difficult to filter out due to their wide frequency bandwidth.

It is necessary to position the scanning subject in the centre of the planar array to have a reference point for the image reconstruction and to have the maximum number of measurements within the subject volume by the acquisition system. Symmetrical and non-symmetrical analysis of the Mk4 planar array is performed to explain the significance from a signal processing point of view.

It is clear from the results obtained that by using 0.3mS/cm dielectric medium will result in a better electric potential mapping being acquired from the subject as compared to 0.5mS/cm and 0.7mS/cm. at the level of 0.3mS/cm, breast tissue has greater impedance and hence will result in a higher potential drop.

In a planar array based system several issues cause the saline to be displaced from the electrode pins resulting in loss of information. This loss of information from the combination of electrodes will comprise the image quality. In this research all the possible factors causing the electrode to block are described in detail and the theory behind them discussed.

Thorough research has been carried out in order to investigate what ratio of electrode blockage will result in information loss. By analyzing the results produced from these air gaps covering different ratios of the driving and receiving electrodes it is concluded that a completely blocked receiving electrode introduces high impedance resulting in a saturated signal. The completely blocked driving electrode will return very low potentials causing the whole frame measurement to be void.

The occurrences of infinite impedance leading to abnormal measurements are mitigated using the following methods.

A software program has been designed in LabVIEW for indicating whole electrode blockage due to tissue or debris effects. This program uses combinations of 50 drive

patterns to determine the high impedance combination by detection of a spike. Further, several experiments are also carried out using different protocols to minimize saline displacement from the electrodes due to skin pressure to suggest the most appropriate solution.

Several experiments are carried out using different protocols to minimize saline displacement from the electrodes. The aim is to use a method that will form a constant saline layer between the subject and the electrode but at the same time produce a response closer to that of the original electrode plate. Protocols used for the experiments include the use of medical ring gauze and ridges.

7.3 Future Work

Bandwidth limitation due to the analogue multiplexer and current source configuration can be overcome by the proposed multiple current sources and multiplexer layout is defined in the block diagrams shown below Figure 7.1 and Figure 7.2 in which the layout of input capacitances C_{ON} ,C_{OFF} and R_{ON} are indicated. The proposed layout will overcome the current bandwidth limitation due to a low pass effect discussed in Chapter 4.

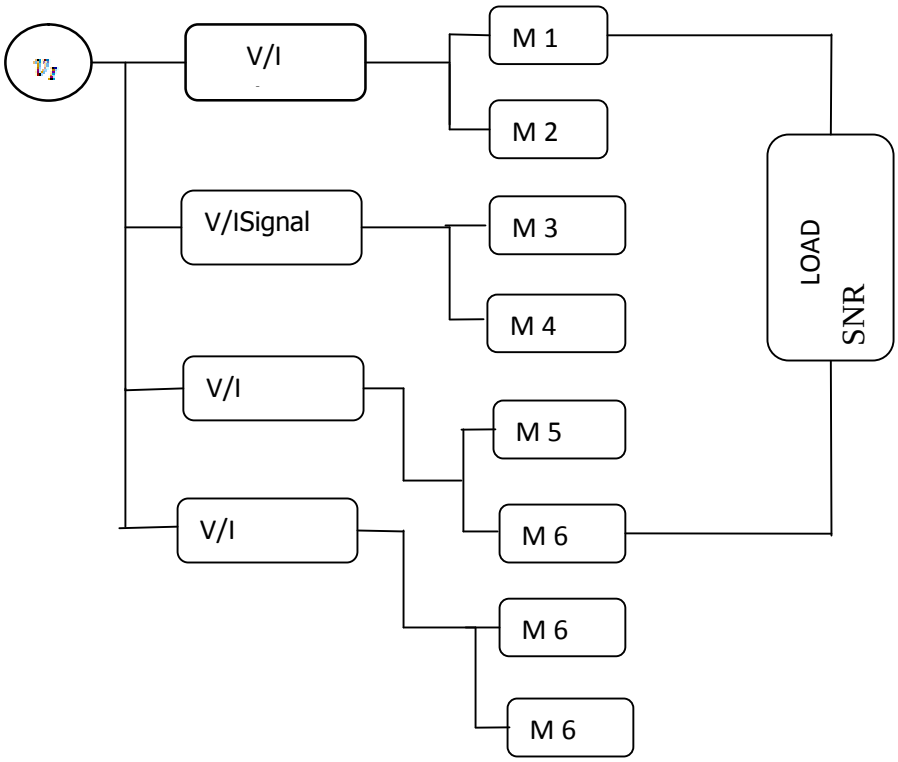

Figure 7.1. Proposed multi current sources layout

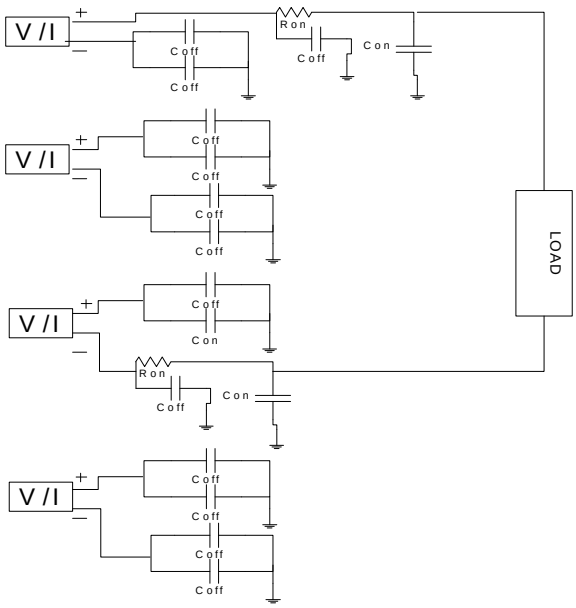

Figure 7.2. Proposed multi current sources layout in terms of multiplexer's capacitance

C_{ON} ,C_{OFF}.

In practice, a high output impedance with the EIT current source is difficult to obtain due to the stray capacitance shunting the output impedance.

It is suggested to use high precision voltage sources (Zhu *et al* 1993, Hartov *et al* 2000) in the Sussex EIM System instead of current sources. Voltage sources with low output impedance will tend to result in the applied voltage remaining unaffected for a wide range of varying load impedances (Saulnier *et al* 2006). A general block diagram representation of a voltage source suitable for the Sussex EIT System is shown in Figure 7.5.

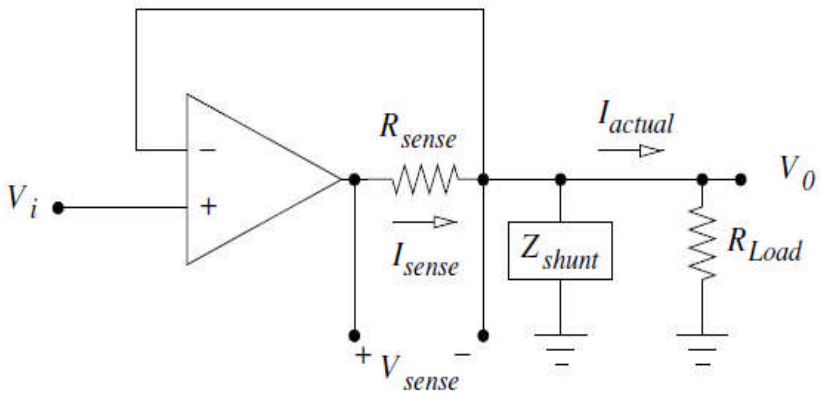

Figure 7.5.Voltage source with current measuring load resistor (Saulnier *et al* 2006)

The possibility of electrode blockage due to the patient's skin is more when the breast is pressed against the electrode plate while scanning the volunteer lying on her front. Thus a proposed change of the scanning position is to have the volunteer lie sideways as this could minimize the breast and electrode plate contact. However, lateral scanning requires further investigation.

By adjusting the scanner head depth 1 or 2mm more than that of the subject's volume can reduce skin and electrode plate contact. This proposal needs complete investigation before implementation. Moreover further investigation is needed into how the existing specific depths are calculated and chosen.

The accuracy of a planar array system depends on the minimization of systematic errors. These errors can be analyzed and then calibrated. The analysis at the current source section will include the optimization and calibration of each current source for output impedance and frequency response with variable loads, the minimization of inter-source phase offset and amplitude. The tests would include development of both hardware and automated test software for the clinical setting.

Calibration of the Sussex EIM System is required periodically to check the performance of the components which may vary with time. The Mk4 System has complex hardware and software sub-systems, which require close coordination. As it is difficult to assess the system performance in vivo, physical, biological and electronic phantoms are required for the calibration procedures.

An electronic phantom can be designed to imitate human tissues to study different resistances and reactances seen from the Sussex planar array based EIM device. Designing of the different models of phantoms based on resistive 3 and 4 element cole-cole models could be simulated in PSPICE software and used for the calibration of individual electrodes and electrode pairs. These electronic phantoms could also be used for gain and phase calibration.

References

American Cancer Society 2009 Breast cancer facts & figures 2009-2010.

BreastNet 2004 Types of breast cancer: http://www.bci.org.au/public/types.htm

Cancer Research UK, http ://www.cancerresearchuk.org

Ferlay, Shin, H.R 2010 GLOBOCAN 2008 v 1.2, Cancer Incidence and Mortality Worldwide : IARC CancerBase NO.10.Lyon,France.

Isard H.,Sweitzer,C.J.,Edelstein 1988 .A prognostic indicator of breast cancer survival ,WILEY,Cancer 62:484-488

Knowles, M.A., Selby, P. 2005 Introduction to the cellular and molecular biology of cancer. Oxford: Oxford University Press.

Margie Patlak, Sharyl J.Nass, I.Craig Henderson and Joyce C, 2001 Mammograhpy and Beyond,Developing Technologies for the Early Detection of Breast Cancer:A non-technical Summary.

Tobias, J.S., Hochhauser, D., Souhami, R.L.C 2010 Cancer and its management. 6th ed. Oxford: Wiley-Blackwell.

Aston R.,1990 Principles of biomedical instrumentation & measurement, Pearson Education POD.

Avis N.J., Barber D.C.1994 Image reconstruction using non-adjacent drive configurations,Physiology.Meas.15 pp.153-160.

Barber D.C., Brown B.H.1982 Applied potential tomography-a new in vivo medical imaging technique, Proc. Hospital Physicists Annual Conference, Sheffield Clinic Phys Physiology Meas.

Barber D.C., Brown B.H., Freeston I.L.1983 Imaging spatial distributions of resistivity using applied potential tomography, Electronic Lett,19(22),pp.933-935.

Barber D.C., Brown B.H., Avis N.J.1992 Image reconstruction in electrical impedance tomography using filtered back projection, in Proc. Annual Int. Conf. IEEE Engineering in Medicine and Biology SOC.,pp.1691-1692.

Brown B.H., Seager A.D.1987 The Sheffield data collection system, Clinical Physics Physiology Meas., vol.8,pp.A:91-97.

Brown B.H., Barber D.C. 1995 Low cost functional imaging-electrical impedance tomography, Engineering in Medicine and Biology Society and 14th Conference of Biomedical Engineering Society of India,pp.1/7-1/8.

Barber D C and Brown B H 1984 Applied Potential Tomography (Review Article). J.Phys. E.: Sci. Instrum. 17 723-733

Béqo N,Sze G, Huber N, Wang W 2010 The flexible and configurable Sussex EIM MK4 using PCI eXtensions for Instrumentation (PXI). Journal of Physics: Conference Series. 224 012164

Béqo N, Huber N, Bilal R, Zhang W, Qiao G, Wang W 2011 Fast method for artefact detection and breast boundary definition Journal of Physics.

Bilal R, Wang W, Young R 2011 Analysis and approach to reduce electrode contact artefacts in EIM IEEE EMS 2011,Madrid-Spain,16-18 Nov,2011.

Bilal R, Beqo N, Khan B, Young R, Wang W 2011 Analysis ,Fast method of detection and approach to reduce electrode contact artefacts in EIM IEEE SCOReD 2011,Putrajay-Malaysia,19-20 Dec,2011.

Boone K G and Holder D S 1996 Effect of skin impedance on image quality and variability in electrical impedance tomography: a model study Med. and Biol. Eng. and Comput. 34 (5) 351-354

Campbell J.H., Harris N.D., Zhang F., Brown B.H. , Morice A.H. 1994 Clinical applications of electrical impedance tomography in monitoring of changes in intra thoracic fluid volumes, Physiology Meas.15,pp.A271-A222.

Cherepenin V.A., Karpov A.Y., Korjenevsky A.V., Kornienko V.N., Kultiasov Y.S. 2002 Three-dimensional EIT imaging of breast tissues: system design and clinical testing, IEEE transactions, Volume: 21, Issue: 6, pp.662-667.

Cole K.S., Cole R.H. 1941 Dispersion and absorption in dielectrics, Journal of Chemical Physics 9, pp.341-392.

Cook R.D., Saulnier G.J., Gisser D.G., Gobble J.C., Isaacson D.1994 ACT3:A high speed, high precision electrical impedance tomography, IEEE Trans. Biomedical Eng.,vol.41,pp. 713-722.

Edic P.M., Saulnier G.J., Cheney M., Isaacson D., Newell J.C., Gisser D.G., Cook R.D. 1993 Implementation of a real time electrical impedance tomography, in Proc. Annual Int. Conf. IEEE Engineering in Medicine and Biology Soc., pp. 84-85.

Edic P.M., Saulnier G.J., Newell J.C., Isaacson D.1995 A real time electrical impedance tomography ,IEEE Trans. Biomedical Eng. Vol.42,pp.849-858.

Foster K.R., Schwan H.P. 1998 Dielectric properties of tissues and biological materials: A critical review, Critical Rev. Biomedical Eng. 17, pp.125-129.

Fricke H., Morse S.1925 The electrical resistance and capacity of blood for frequencies between 800 and 4.5 million cycles, J.Gen. Physiology, Vol.9, pp.153-167.

Gabriel C, Gabriel S.1996 Compilation of the dielectric properties of body tissue at RF and microwave frequencies, AL/OE-TR-1996-0037.

Gisser D.G., Isaacson D, Newell J.C.1988 Theory and performance of an adaptive current tomography system, Clinic Phys. Physiological Measures, Vol 9,sup. A, pp.35-41.

G Sze, N Beqo, N Huber.Signal Calibration for an Electrical Impedance Mammography System. Journal of Physics: Conference Series 224(2010)012168.

Gongalves S.I., Jan C., Jeroen P.A. June 2003 In vivo measurements of the brain and skull resistivities using an EIT based method and realistic models for head, IEEE Transactions on Biomedical Engineering,Vol.50,No.6.

Hartov A., Mazzarese R.A., Reiss F.R., Kerner T.E., Ostermann K.S., William D.B., Paulsen K.D 2000 A multichannel continuously selectable multifrequency electrical impedance spectroscopy measurement system, IEEE Transactions on Biomedical Engineering 47(1),pp. 49-58.

Henderson R.P., Webster J.G 1978 An impedance camera of spatially specific measurements of the thorax, IEEE Trans BIOMED. Eng. 25(3), pp.250-254.

Holder D.S.1992B Electrical impedance tomography with cortical or scalp electrodes during global cerebral ischemia in the anaesthetized rat, Clinic Phys. Physiology Meas., Vol. 13,No.1,pp.87-98.

Holder D.S 1993 Clinical and physiological applications of electrical impedance tomography, London, U.K, UCL Press.

Holder D S 2004 Electrical Impedance Tomography: Methods, History and Applications, (London: Institute of Physics) ISBN 0-7503-0952-0

Henderson R P and Webster J G 1978 An Impedance Camera for Spatially Specific Measurements of the Thorax IEEE Trans. Biomed. Eng. 25: 250-254

Han, Yang, Frazier, A.B. 2007 Quantification of the heterogeneity in breast cancer cell lines using whole-cell impedance spectroscopy. Clinic Cancer Res, 13 (1), 139-43.

Hua P, Woo E J , Webster J G,Tompkins W J 1993 Finite element modelling of electrode-skin contact impedance in electrical impedance tomography IEEE Trans. Biomedical Engineering 40 (4) 335-343.

Huber N, Béqo N, Adams C, Sze G, Tunstall B, Qiao G , Wang W 2010 Further investigation of a contactless patient-electrode interface of an Electrical Impedance Mammography system. Journal of Physics: Conference Series 224 012166

Impedance tomography, Retrieved from internet 2004: http://butler.cc.tut.fi/~malmivuo/bem/bembook/26/26.htm.

Jossinet, J. 1996 Variability of impedivity in normal and pathological breast tissue. Medical and Biological Engineering & Computing,34 (5), 346-50.

Kim H.C., Moon D.C., Kim M.C., Kim S., Lee Y.J 2002 Improvement in EIT image reconstruction using genetic algorithm, Proceedings of the 2002,Vol. 5,pp. 3858-3863.

Mcadams E.T., Jossinet J 1995 Tissue impedance: An historical overview, Physiological Measurement 16(3A).

Medical Imaging Research Electrical impedance tomography, Retrieved from internet 2004 :http://www.geocities.com/capecanaveral/9710/eit.html.

McEwan, A., Romsauerova, A., Yerworth, R., Horesh, L., Bayford, R. & Holder, D. 2006 Design and calibration of a compact multi-frequency EIT system for acute stroke imaging. Physiological Measurement, 27 (5), S199-S210.

McEwan A,Cusick G, Holder D S 2007 A review of errors in multifrequency EIT instrumentatio Physiol. Meas. 28 197-215

Nopp P., Zhao T.X., Brown B.H., Wang W 1996 Cardio-related changes in ling resistivity as function of frequency and location obtained from EITS images, Physiology Meas.17,pp.213-225.

Ryan J.Halter, Alex Hartov, Keith D.Paulsen 2008 A broadband High Frequency Electrical Impedance Tomography System for Breast Imaging. IEEE Transaction on Biomedical Engineering, Vol.55, No.2.

Saulnier G.J., Blue R.S., Newell J.C., Isaacson D., Edic P.M. 2001 Electrical impedance tomography, IEEE signal processing magazine.

Seagar A.D., Baber D.C., Brown B.H 1987 Theoretical limits to sensitivity and resolution in impedance imaging Clinic Phys. Physiology Meas. 8,pp 13-31.

Sinton A.M., Smith R.W., Mcardle F.J., Brown B.H 1992 Fast display for real time electrical impedance tomography, Proc. Annual Int. Conf. IEEE Engineering in Medicine and Biology Soc.,pp.1708-1709.

Smith R.M., Brown B.H., Freeston I.L., Mcardle F.J., Barber D.C 1990 Real time electrical impedance imaging, Proc. Annual Int. Conf. IEEE Engineering in Medicine and Biology Soc.,pp.104-105.

Smith, S.R., Foster, K.R. & Wolf, G.L 1986 Dielectric properties of VX-2 carcinoma versus normal liver tissue. IEEE Trans Biomed Eng, 33 (5), 522-4.

Surowiec, A.J., Stuchly, S.S., Barr, J.B. & Swarup, A. 1988 Dielectric properties of breast carcinoma and the surrounding tissues. IEEE Trans Biomed Eng, 35 (4), 257-63.

Sze G, Wang W, Barber D C , Huber N Preliminary study of the sensitivity of the Sussex Mk4 Electrical Impedance Mammography planar electrode system Journal of Physics: Conference Series 224 012167

Tidswell, A.T., Gibson, A., Bayford, R.H. & Holder, D.S.2001 Validation of a 3D reconstruction algorithm for EIT of human brain function in a realistic head-shaped tank. Physiological Measurement, 22 (1), 177-85.

Towers CM.M, Mccann H., Wang M 1999 Simulation of EIT for monitoring impedance variations within the human head, Biomedical applications of EIT Conf.

Wang W et al 2007 Study into the repeatability of the electrode-skin interface utilizing electrodes commonly used in Electrical Impedance Tomography IFMBE Proceedings, ICEBI 2007 17 (10) 336-339

Zhao T.X.,Brwon B.H.,Nopp P.,Wang W.,Leathard A.D., Lu L 1996 Modelling of cardiac related changes in lung resistivity measured with EITS, Physiology Meas. 17,pp.227-234.

Zhu Q.S., Mcleod C.N., Denyer C.Q., Lidgey F.J., Lionheart W.B 1994 Development of a real time adaptive current tomography, Physiology Meas., Vol. 15,sup. 2A,pp 37-45.17,pp.227-234.

Zou Y and Guo Z A 2003 A review of electrical impedance techniques for breast cancer detection.